Fatigue assessment of welded joints using the sub-modelling technique

João Paulo de Matos Patinho Milheiro

Thesis to obtain the Master of Science Degree in

Mechanical Engineering

Supervisors: Prof. Virgínia Isabel Monteiro Nabais Infante

Prof. Catarina Isabel Silva Vidal

Examination Committee

Chairperson: Prof. Luís Filipe Galrão dos Reis

Supervisor: Prof. Virgínia Isabel Monteiro Nabais Infante

Member of the Committee: Prof. Ricardo Miguel Gomes Simões Baptista

November 2018

Abstract

The fatigue phenomenon has proven to be one of the main causes of failure in mechanical and structural components. Fatigue design and evaluation is nowadays an essential field in engineering, that needs constant innovation to allow for ambitious projects to be carried out ensuring that the safety margins are met.

In the present work, the numerical results are combined with a standard based on experimental results and with analytical extrapolation techniques. The extrapolation methods can use different kinds of analysis outputs such as the linearization of bending and membrane stresses or a range between the maximum and minimum principal stress values. A fatigue assessment was performed in 3 different geometries where 3 attachments are welded with different arrangements. In a first step, the most demanding load was identified from among the 7 available and was then used to make the comparison of the geometries in terms of stress range on the weld details. The analysis was repeated for each critical point of the weld and the results were post-processed, according to the standard proposed by ITER (EN-13445-3). A ratio between the number of cycles, N_E assigned to the components and the maximum allowed stress cycles, N_{max}, is translated in the project safety margin.

The structure has dozens of components to be assessed and all arrangements proposed that respect the system constraints were thus valid. It is expected that there will not be experimental values to compare with the numerical results. On the other hand, the results obtained for the third geometry agree with the project safety criteria and applicable standard. In the third geometry, the welded connections were placed further away from each other and in less demanded areas in terms of stress. The stress range decreased about 25% in one of the weld details and 40% in the other, complying with the safety coefficient, n = 20, required.

Keywords: Fatigue assessment, stress range, hot-spot stress, weld, Ansys®.

Resumo

O fenómeno da fadiga provou ser uma das principais causas de falha em componentes mecânicos e estruturais. O projeto e análise à fadiga é uma área essencial na engenharia atualmente que necessita de constante inovação para permitir que sejam desenvolvidos projetos ambiciosos, assegurando que as margens de segurança são cumpridas.

No presente trabalho, os resultados numéricos são combinados com uma norma baseada em resultados experimentais e com técnicas de extrapolação analíticas. Estes métodos podem usar diferentes tipos de resultados numéricos, tais como a linearização de tensões de membrana e flexão ou a diferença entre os valores de tensão principal máxima e mínima. Foi realizada uma análise de fadiga em 3 geometrias diferentes onde são soldados 3 apoios com disposições diferentes. Numa primeira fase, os 7 carregamentos disponíveis são comparados para identificar o mais exigente para os componentes e foi de seguida usado para comparar a amplitude de tensões resultante na soldadura nas 3 geometrias. A análise foi repetida para cada ponto crítico da soldadura e os resultados foram processados de acordo com a norma EN 13445-3, proposta pelo ITER. A margem de segurança do projeto é obtida analiticamente pela relação entre o número de ciclos de fadiga exigido aos componentes, N_E, e o número máximo de ciclos de fadiga permitidos.

A estrutura tem uma grande quantidade de componentes soldados para serem analisados e todas as disposições propostas que respeitem os requisitos do sistema são válidas. É esperado que não existam resultados experimentais para comparação com os resultados numéricos. Por outro lado, os resultados obtidos com a terceira geometria respeitam os critérios de segurança do projeto e a norma aplicada. Na terceira geometria, as uniões soldadas foram colocadas mais afastadas umas das outras e em áreas que apresentam valores mais baixos de tensão. A amplitude de tensão registada diminuiu 25% numa das zonas da soldadura e 40% noutra, cumprindo o coeficiente de segurança, n = 20, exigido.

Palavras-chave: Análise de fadiga, gama de tensões, tensão *hot-spot*, soldadura, Ansys®.

Contents

List of tables

List of figures

Glossary

ITER	International Thermonuclear Experimental Reactor
VV	Vacuum Vessel
LCF	Low-cycle fatigue
HCF	High-cycle fatigue
FEA	Finite Element Analysis
FAT	Weld S-N curve classification
APDL	Ansys® Parametric Design Language
CAD	Computed Assisted Design
ID	Identification
UF	Usage factor
EM	Electro-Magnetic

Nomenclature

W	Total load applied to train axle
a	Crack length
N	Number of fatigue stress cycles
N_E	Number of fatigue stress cycles required
N_{max}	Maximum number of fatigue stress cycles allowed
N_n	Number of fatigue stress cycles during the crack nucleation
N_p	Number of fatigue stress cycles during the crack propagation
ΔK	Stress intensity factor
ΔK_{th}	Threshold value of the stress intensity factor
ΔK_c	Critical value of the stress intensity factor
C, m	Constants in Paris Law determined experimentally
σ	Normal stress
σ_{nom}	Nominal stress
σ_{mem}	Membrane stress
σ_{ben}	Bending stress
σ_{nlp}	Non-linear peak stress
σ_y	Yield stress
σ_a	Fatigue stress amplitude
σ_m	Fatigue mean stress
σ_{min}, σ_{max}	Minimum and maximum stress value
$\Delta\sigma$, S_r	Stress range
$\Delta\sigma_n$	Nominal stress range
$\Delta\sigma_{hs}$, σ_{hs}	Hot-spot stress range
σ_{peak}	Stress peak value
R	Stress ratio
S_f	Fatigue strength

S_{ut}	Ultimate stress
S'_e	Fatigue endurance limit of specimen
S_e	Fatigue endurance limit of real component
k_a, k_b, k_c, k_d, k_e, k_f	Correction factors to apply to the fatigue endurance limit of specimen
F	Applied force
M	Applied bending moment
V	Transverse load
H	Tensile load
t, e_n	Base material thickness
t_p	Attachment thickness
r, r_m	Weld radius match
θ	Weld geometry angle
L_0	Initial length
ΔL	Length increment
E	Young's Modulus
ρ	Density
α	Coefficient of thermal expansion
K	Thermal conductivity
C_p	Specific heat
T_{min}, T_{max}	Maximum and minimum temperature value
T*	Mean temperature value
f_{T^*}	Temperature correction factor
f_{ew}	Thickness correction factor
$\Delta\sigma_{corr}$	Corrected hot-spot stress range

1 Introduction

1.1. Framework

The growth of applications in the field of engineering allied with the need to guarantee gains in economic efficiency has been leading to further studies in the area of the mechanical behaviour of materials under certain service conditions, namely problems related to fatigue and fracture in the sense of extending the useful life of the equipments and avoid mechanical failures. Failures due to fatigue in welded structures lead to a reduction in life and substantial costs each year all over the world.

The components in structures and machines are subjected to variable loads and require to be dimensioned according to criteria that can guarantee its reliability and durability. A decrease in the number of fatigue failures can be achieved by introducing various standards and fatigue design standards, that are based on rigorous experimental tests. In practice, there is a diversity of project requirements that can be difficult to represent on an experimental level. The loads can, for example, be applied abruptly or slowly, defining the frequency of the fatigue cycles, the environment can have corrosive characteristics and the surrounding temperature can be constant or have a transient character. Manufacturing processes, including the permanent connection processes like welding introduce other variables that determine, together with the base materials' properties, the properties of the final component. Examples of this variables are the appearance of residual stresses and the existence of a heat affected zone.

The propagation of fatigue cracks can occur in conditions with low nominal stress levels, if it has a cyclic or variable nature. However, the crack nucleation process occurs more frequently in critical areas of the material such as the presence of a notch or in areas with an abrupt change in the component's section, where the stress concentration is greater.

The difficulty of performing experimental tests to all the components in different positions and with distinct shapes requires the utilization of numerical methods to design all the elements with the required safety factors. The fatigue criteria are based, in some cases, on old concepts that do not easily translate the output from modern computer programmes and are also limited to rather simplified structures. The challenge is then to create modern standards that prove to be adaptive and embracing, to be combined with the numerical solutions.

The materials' fatigue is nowadays a very important field in research. The concern with this theme started in the XIX century with episodes like the Versailles train crash and the first work on this matter was presented in 1867 by August Wohler, based on that crash [1]. A large part of these components had a short lifespan against the expected, when designed according to static endurance criteria. The critical component that lead to the crash was the train axle. The failure occurred under normal loading conditions without marks of plastic deformation, although they have been tested previously and revealed a good ductility. From the mechanical point of view,

the situation was equivalent to consider a beam under load in 4 different points, like represented in figure 1.1, where W is the total load applied in the axle due to weight.

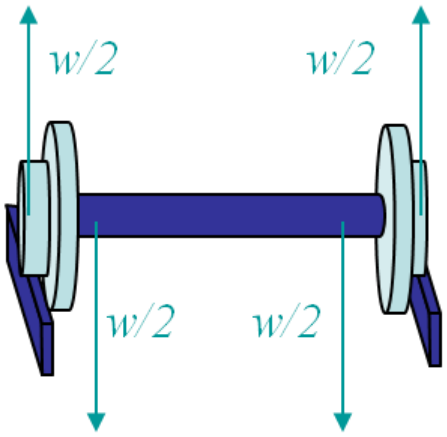

Figure 1.1 - Representation of loads in a train axle [2]

This arrangement of loads produce compressive stresses in the upper section of the axle and tensile stresses in the lower section of the axle. After half revolution of the axle, the stress values are inverted and the induced load behaviour has a sinusoidal behaviour. The study of this case leaded to a lot of knowledge on this area, including the S-N curve.

1.2. Objectives

This study aims to contribute for the design of components of a reflectometry system to be installed in the interior of a vacuum vessel of ITER, an experimental reactor of nuclear fusion. This system includes antennas, wave guides and other components for detailed measurements that are bolted to bosses, welded to the vacuum vessel inner shell. The welded joints required for this are the target of this fatigue assessment that needs to follow the standard EN-13445-3 [3], developed in France specifically for weld details of pressure vessels.

The fatigue assessment is carried out using finite element analysis with the software Ansys ® and resorts to numerical tools like the sub-modelling technique and analytical tools like extrapolation methods for the stress values. The main objectives are to validate the application of these tools in this kind of study and to obtain a geometry that meets the design requirements within the safety margins imposed. The work was divided in the following 3 main steps:

- Evaluate the static results of each load case scenario to be applied in the structure;
- Improve the initial geometry provided by ITER until the safety condition required is met in all the critical weld point, using worst load case scenario as setup;
- Calculate the total safety coefficient of the project, considering all the load cases.

1.3. Thesis structure

The present essay is divided in 6 chapters and has the following organization:

In chapter 1, a brief introduction is made to the difficulties that are faced nowadays when designing components and the motivation to choose this topic, the main objectives of this study and the structure of the thesis are described.

In chapter 2, the theoretical bases to this study are discussed in order to have a solid starting point for the fatigue assessment. The principal characteristic of the fatigue process like phases that constitute it until the mechanical failure occurs, the different types of fatigue depending on the intensity of the loads and other aspects that can influence it are described. A summary of this topic concerning the welded joints is also made and the stress extrapolation methods available that can be used later on the dissertation are explained individually.

In chapter 3, the case study is presented. It includes the description of the initial geometry provided, the physical meaning of the different load scenarios and the problem that in intended to be solved.

In chapter 4, a description of the software used and the methodology behind the finite element simulations and the post-processing of the results. The 2 geometrical improves and the advantages that each one should bring to achieve the objectives are explained, just like the material used in the whole structure and the technical specifications of the loads. The chapter also includes the explanation of the procedures to organize the information provided in external files and used as load input in the analysis, the mesh technique and the analysis setup.

In chapter 5, the results obtained from the analysis are compared and commented to check that the objectives proposed are met. The comparison of the static results that each load scenario creates in the structure are described and the most harmful load is chosen for the next step of the assessment. The improvements in the safety factor resulting from the different boss arrangements is described. The total safety factor that was achieved in this work is compared with the requirements.

In chapter 6, the conclusions of the results compared in chapter 5 are presented and some future works that will help to complete and improve this study are described.

2 State of Art

2.1. Fatigue

Mechanical fatigue of materials is a process of localized degradation that occurs in structures subject to stress and consequently deformation variations. The resulting damages are progressive and permanent and produce the nucleation and propagation of cracks or the fracture if the mechanic limit of the material is reached. The failure by fatigue does not happen because the loads applied are too high but because a critical number of cyclic repetitions is achieved. Many static failures give a visible warning in advance, but a fatigue failure gives less warning. It is sudden and total [4].

Some years ago, it was common in engineering to design components only considering the material's yield stress criterion, with the purpose of avoiding any permanent deformation in the structure. For conservative reasons, the allowable stress to consider in the project is then the yield stress divided by a safety factor that can be related to the material type, the loads type, the severity of the failure, etc.

When studying or designing components for fatigue, the most important stress parameter to consider is the stress amplitude between the maximum and minimum value applied in the components. The ultimate and yield stress values are also important but loads in this range would make the structure fail first statically without the need of stopping and re-applying the loads. In other words, failure would be verified before the fatigue process happens or after a very small number of fatigue cycles.

2.1.1. Characterization of the fatigue process

The fatigue mechanism consists on several cyclic deformations of the material that even being microscopic, are not totally reversable and will lead to its instabilization and failure after an amount of cycles. This occurs along sliding planes in the contour of the grains that constitute the material or around irregularities caused by geometrical and composition defects.

The whole process since the first load is applied until the component fail by fatigue can be divided in three different phases [5]:

- The first phase consists in the nucleation of the fatigue crack. During this period there is no crack of any length in the component and it is not noticeable where it will appear. Due to the deformations that the material suffers and recovers partially or totally, its properties change and a crack can initiate in the critical areas. This phase can represent more than 90% of the structure life because it is when the components still have the original shape, but it can be reduced by the presence of pre-existing defects;

- The second phase starts when the crack appears and consists in its growth and propagation, reducing the area of material that is supporting the loads;
- In the last phase of the fatigue process is when failure occurs. This happens because the remaining material cannot hold the loads that even being low, are applied in a small cross section, so the components gets instable and breaks. Failure always shows a brittle fracture regardless of whether the material is brittle or ductile.

The fatigue crack propagation phase can be divided in three stages that are represented in figure 2.1. The variable in the horizontal axis is the stress intensity factor and in the vertical axis is the speed of the crack propagation based on the number of fatigue cycles applied. In the first and third stages the propagation in unstable and unpredictable, so it can only be studied in the second stage.

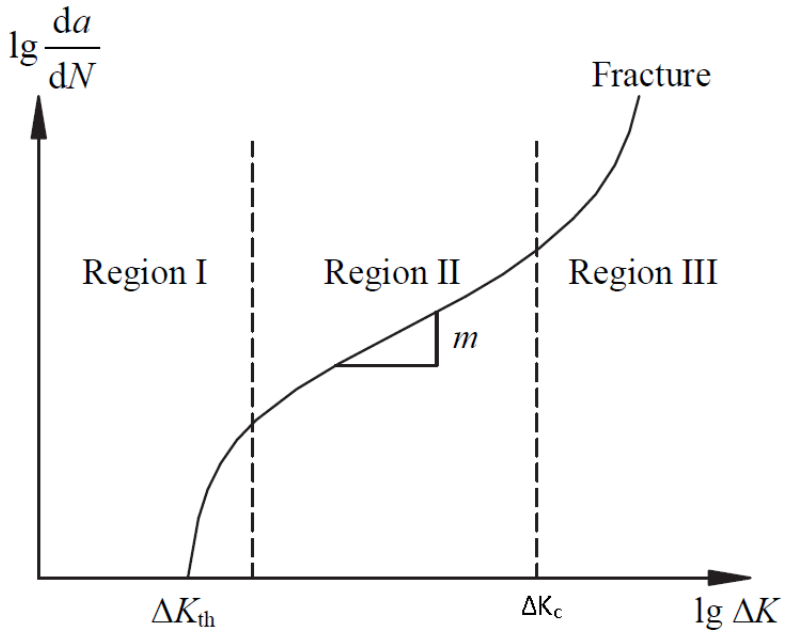

Figure 2.1 - Fatigue crack grow rate [6]

In the first region of the graphic can be identified the threshold value of the stress intensity factor ΔK_{th} necessary for the crack to appear in the component and this stage of the fatigue process start. The frequency that the stress cycles are applied is always constant and the crack length (a) grow rate, depending on the number of cycles (N), increases exponentially until it stabilizes and stage 2 starts. Here the crack grow rate can be described with the Paris law in equation (2.1), where C and m are a material properties and ΔK_c is a critical value for the stress intensity factor [7].

$$\frac{da}{dN} = C\Delta K^m, \Delta K_{th} < \Delta K < \Delta K_c \quad (2.1)$$

As the crack grows, the area of material supporting the loads gets smaller and the stress concentration factor increases. After ΔK_c is achieved, the crack propagation becomes unstable and its length increases exponentially. After a short time, the thirst stage of the fatigue process mentioned before is reached and the component's fatigue life ends.

2.1.2. Fatigue life prediction

The last phase of the fatigue process is practically instantaneous, so the total number of cycles (N) that occur during the fatigue life of the components can be given by the sum of the number of cycles in the crack nucleation phase (N_n) and the number of cycles in the crack propagation phase (N_p) [8], as equation (2.2) shows.

$$N = N_n + N_p \tag{2.2}$$

The physical effect of a repeated load on a material is different from a static load [5]. Figure 2.2 shows a fracture by fatigue where the three phases mentioned before can be identified. The first phase is the one that usually takes more time in the process, but is just represented in the bottom of the component cross section as a line or a dot because the crack has not been initiated yet. The small area that starts in the bottom corresponds to the fatigue crack propagation and the surface is smooth because the propagation is relatively slow and the material deformation is ductile. The bigger area on top shows the fast and brittle fracture that happens in phase 3 and because it is not slow and progressive like in phase 2, the fracture surface is rough and easily distinguishable from the rest.

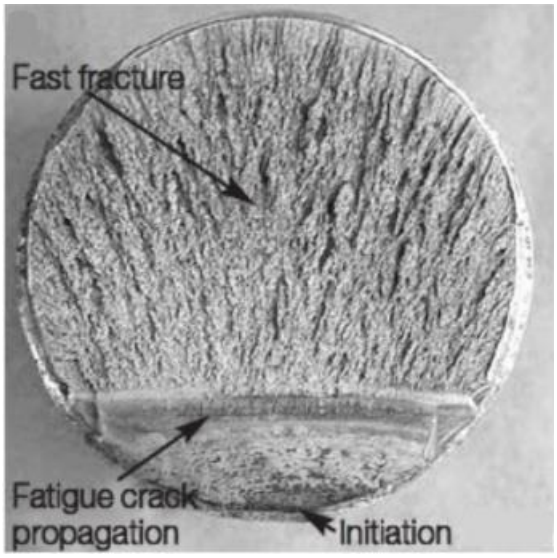

Figure 2.2 - Fracture by fatigue [9]

The size of these 2 areas on the fracture surface can help to understand the intensity of the loads applied. The bigger the area corresponding to the crack propagation is (bottom area in figure 2.2) compared to the fast fracture surface, the lower the stress on the components is because it is harder for the component instabilize and the crack will have to grow during more time and through a longer length, resulting in a smaller area of fast fracture [9].

2.1.3. Fatigue stress cycles

The stress applied repeatedly on a structure can be categorized in two main types: stress cycles with a constant range or amplitude and stress cycles with variable range over the time. This assessment was performed with distinct loads but all of them have a constant stress amplitude, so only the first kind will be explained here.

The stress variation, frequency, range and medium value over the time can be represented generically in a graphic as shown in figure 2.3.

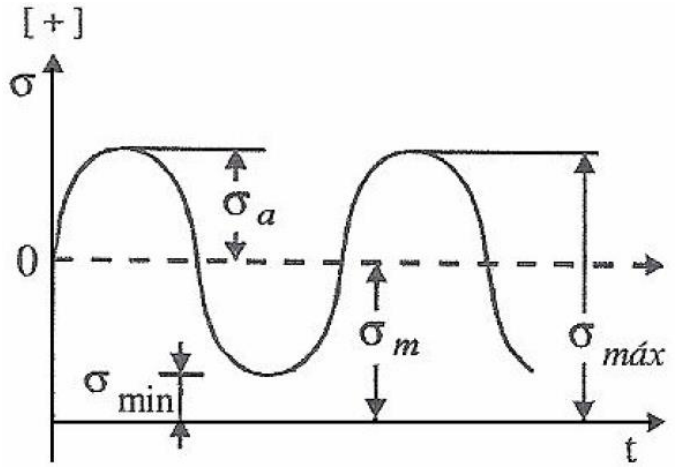

Figure 2.3 - Constant fatigue stress amplitude[10]

$$\sigma_m = \frac{\sigma_{min} + \sigma_{max}}{2} \tag{2.3}$$

$$\sigma_a = \frac{\sigma_{max} - \sigma_{min}}{2} \tag{2.4}$$

Where σ_{min} and σ_{max} are the minimum and maximum value of stress observed cyclically during the fatigue load, σ_m is the medium value (mean stress) between the peak and valley values and σ_a is the amplitude of the stress value that is applied in each stress cycle with positive and/or negative values.

The range between the highest and lowest stress applied is given in equation (2.5).

$$\Delta\sigma = \sigma_{max} - \sigma_{min} = 2\,\sigma_a \tag{2.5}$$

Equation (2.6) gives the stress ratio expression.

$$R = \frac{\sigma_{min}}{\sigma_{max}} \tag{2.6}$$

For the same values of σ_m and $\sigma_a$it is possible to have different values of R and it describes the type of fatigue loading [10]:

- R = 0 means that the load is pulsing, so it varies from 0 to a tensile load with positive values;
- R = -1 means that it is a pure alternating cycle, so the load changes from tensile to compressive;
- R > 0 means that it is a fluctuating cycle, so both stresses σ_{min} and σ_{max} are a tensile load with positive value.

Figure 2.4 has a representation for each of the 3 stress cycles, in the order they were explained

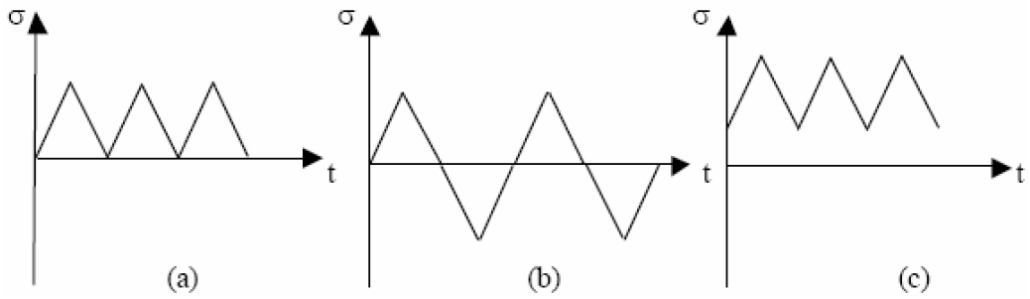

Figure 2.4 - Fatigue cyclic with (a) pulsing, (b) alternating, (c) fluctuating load [10]

2.1.4. Fatigue design

To perform a fatigue design or analysis, 3 different type of fatigue life methods can be used [4].

The first one is the Stress-Life method and relates the stress values measured in the components with the number of cycles the components can take until the mechanical failure is achieved.

The second method is the Strain-Life method and relates the deformation peaks measured in real-time while the loads are applied with the number of cycles performed until the failure.

The last method is called the Linear-Elastic Fracture Mechanics Method and it focus more on the phase 2 of the fatigue process, relating the number of cycles allowed before mechanical fault with the velocity and other parameters of the crack propagation.

2.2. Wohler curves

The “Stress-Life” method presented before is the one followed in this study, because of the proceeding of the standard that is followed, so it will be explained here in more detail. It is applied based on reference values that are obtained from experimental tests. To determine the strength of materials under the action of fatigue loads, specimens are subjected to repeated or varying forces of specified magnitudes while the cycles are counted until the failure occurs.

All the information obtained can be organized in a graphic called the S-N curve or the Wohler curve. August Wohler lived in the XIX century and was the first person to use this kind of scheme, represented in figure 2.5, to relate the loads applied in metal structure with the number of cycles in 1867 [1]. To establish the line visible in the graphic, a fatigue test must be performed at each stress value in order to obtain the corresponding value of stress cycles number (N) allowed. Every test should be repeated several times because of the statistical nature of mechanical fatigue, especially for the strength values where the graphic slope changes because those are important reference parameters in the fatigue design.

The values on the vertical axis of a Wohler curve are properties of the material and are called strength values. Those will be compared with the stress values evaluated in the components being designed or studied to predict the fatigue behaviour.

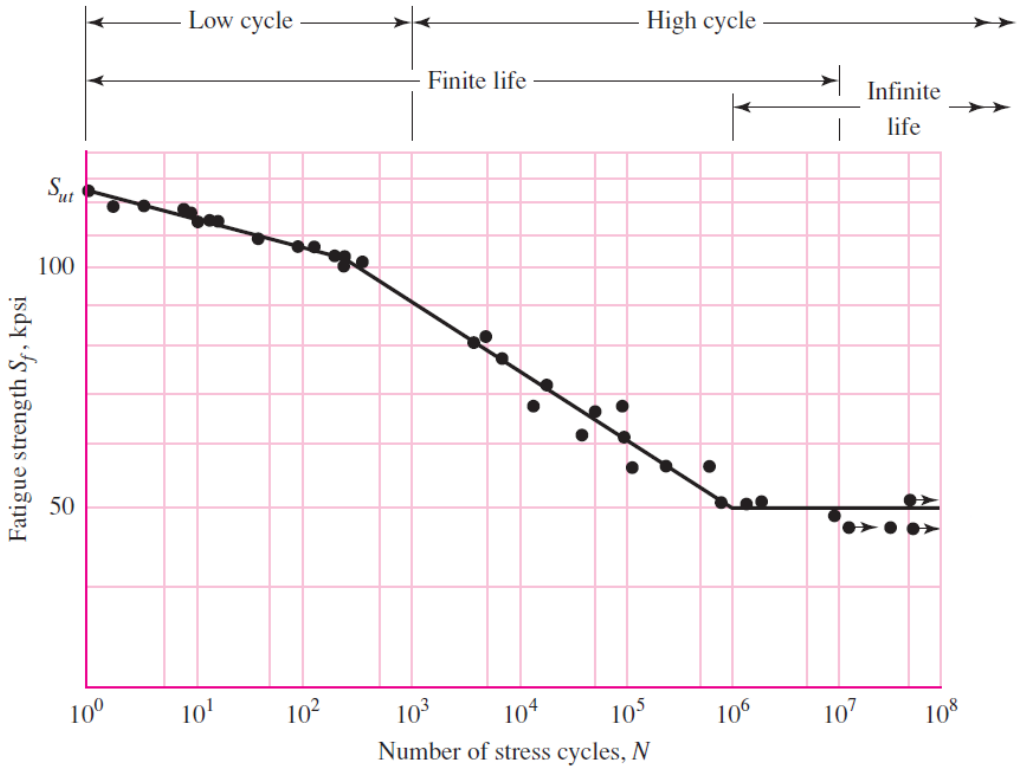

Figure 2.5 - S-N curve [4]

The relationship between stress level and number of cycles to failure in a S-N curve is not linear, which has very important implications for fatigue life. Figure 2.6 shows the difference between using the axis of a S-N curve in linear or logarithm scale.

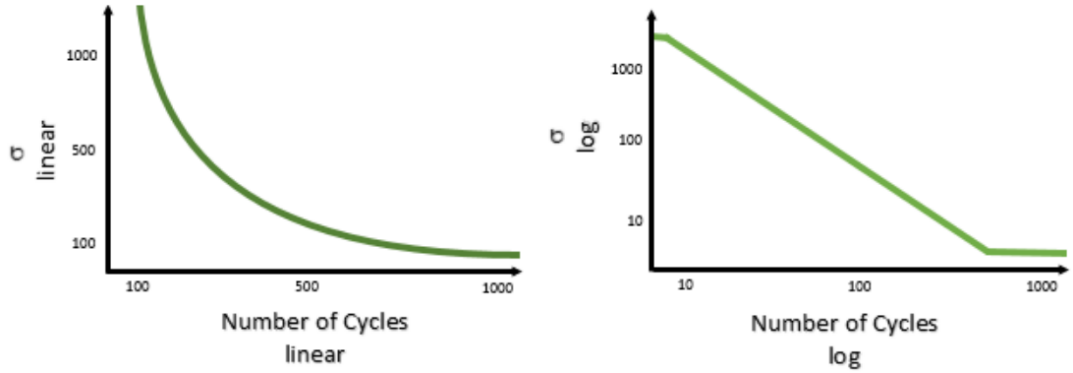

Figure 2.6 - Wohler curve with (a) linear scale, (b) logarithmic scale [11]

The value of the parameter σ_m introduced before has an effect in the S-N curve. Depending on the load conditions, σ_m can have 3 type of values:

- If $\sigma_m = 0$ the minimum and maximum loads applied cyclically are symmetric. This will be considered as the S-N curve reference;
- If $\sigma_m < 0$ the load creates a compressive stress in the structure that increases the number of cycles to failure. The component will break later than the S-N curve with mean stress of zero would predict;
- If $\sigma_m > 0$ the load creates a tensile stress in the structure that reduces the number of cycles to failure. The component will break sooner than the S-N curve with mean stress of zero would predict.

Typically, the S-N curves are developed for a specific mean stress (σ_m) and a variation in this value will shift the curve downward or upward, as figure 2.7 illustrates.

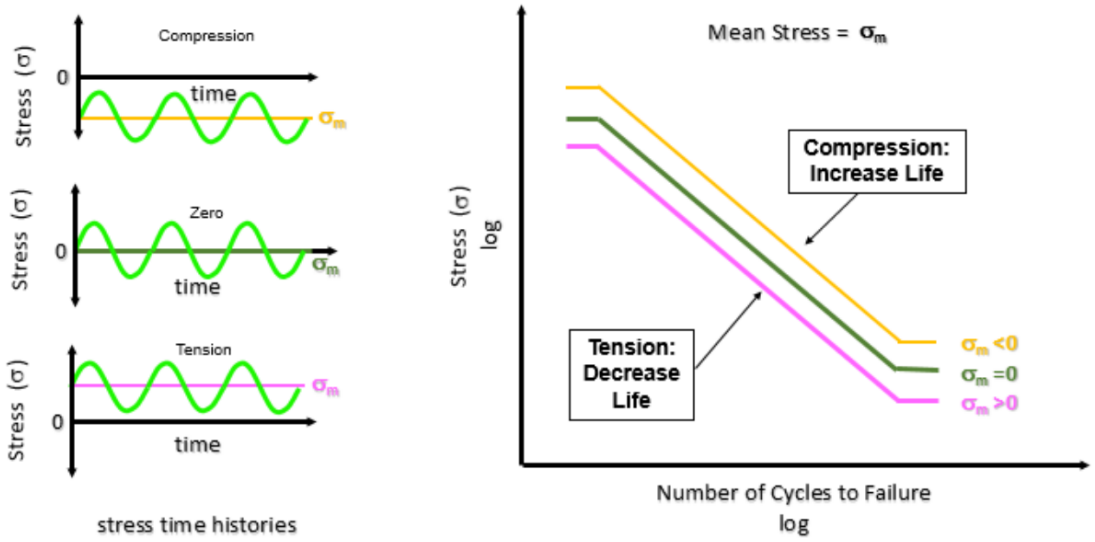

Figure 2.7 - Influence of mean stress on S-N curve [11]

It is also visible in figure 2.5 that the Wohler curve is divided in 2 main parts: low-cycle fatigue and high-cycle fatigue. The way to approach a fatigue assessment is different for each of these fatigue process types.

2.2.1. Low-cycle fatigue

The low-cycle fatigue (LFC) can also be called oligociclic and is characterized by having a number of stress cycles until the failure under 10^3 ~10^4 cycles, depending on the material. This does not mean that the components break within a short period of time because the frequency of the loads can be low, so it takes a long time to apply a small number of cycles. It is visible in figure 2.5 that this range of cycles before the failure corresponds to the first section of the S-N curve where the fatigue strength is higher. For any material, the loads applied in this kind of fatigue process are between the ultimate stress and around the yield stress. The ultimate stress is represented in figure 2.5 as S_{ut} and is the necessary load to fracture the components statically without the application of a cyclic fatigue process. The fatigue strength at the transition to high-cycle fatigue corresponds to the yield stress of the material, what means that the deformations under high-cycle fatigue are mostly plastic, what makes the process faster.

While in low-cycle fatigue the stress is high enough for plastic deformation to occur, the accounting of the loading in terms of stress is less useful and the strain in the material offers a simpler and more accurate description [12]. In figure 2.8 the irreversibility of the transformations is explained. While the load applied belongs in the linear section of the graphic, it is lower than the yield stress, so all the deformation will disappear and the structure returns to its initial shape. When the stress enters the plastic domain between the yield and the ultimate stress and then unload, the graphic follows the straight line parallel to the elastic domain shown before and a permanent plastic strain is visible in the end. This deformation value is now part of the component's permanent dimension and will be the starting point when the load is reapplied and figure 2.8 shows that loads above the highest stress reached before, will create more plastic deformation on the geometry, accelerating more the fatigue process.

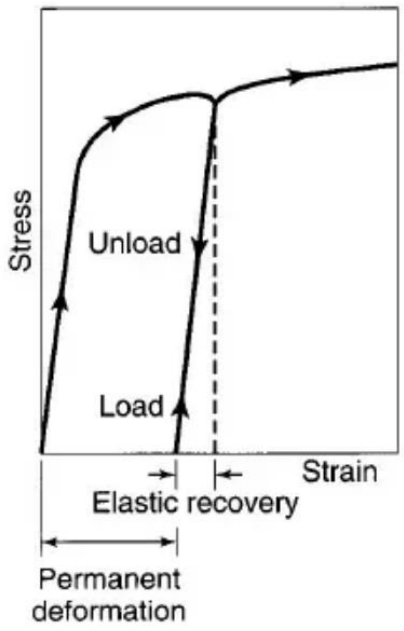

Figure 2.8 - Residual stress after unload [13]

These strain values displayed are amplified for better understanding, but this process happens a lot of times (N times) in a smaller scale until a crack appears and starts to propagate.

The strain-life method mentioned before, also called fatigue controlled by cyclic deformations is the appropriate tool to assess the component's life when the stress is high enough to lead to significant plastic deformations in the areas of stress concentrations [10].

2.2.2. High-cycle fatigue

In the high-cycle fatigue (HCF), the number of stress cycles necessary to achieve the fracture is higher than 10^3 ~10^4 cycles, depending on the material. It is characterized by relatively low applied loads and under the yield stress that represents an upper limit [12], which allows the material to undertake much higher stress cycles, as desired in the fatigue design.

Since the deformations are elastic what is visible in figure 2.8 does not apply in this case, so after each cycle when the structure is loaded and unloaded any permanent deformation is obtained. The stresses are in the elastic domain, but locally and microscopically the material deforms in a plastic and permanent way [5], leading to the possible future cracks. Given this, when a crack is initiated and starts to propagate, the components has its original dimension when observed with naked eye. This is one of the reasons that make the fatigue dangerous and unpredictable.

2.2.3. Endurance limit

The high-cycle fatigue section visible in figure 2.5 shows a section in the end where the graphic turns horizontal that corresponds to the infinite fatigue life of the components. The horizontal line occurs at a stress value called the endurance limit (S_e), that is a stress amplitude below which the material never fails, no matter how large N is. In other words, when designing components for infinite life, the resulting stress amplitude values must be lower than the endurance limit [5]. The number of cycles when the endurance limit is reached depends on many factors like the material and the surface quality but is usually around 10^6 ~10^7 cycles.

This does not happen in all the materials. Non-ferrous metals and alloys like the aluminium, for example, do not have an endurance limit under which the structure is ensured to have an infinite life. Figure 2.9 shows a comparison between the S-N curve of a steel represented with the letter 'A' and the S-N curve of the Aluminium represented with the letter 'B'. This parameter is properly defined for the steel and in the aluminium case the slope of the curve can decrease for values of N over 10^7 cycles [14], so a large value of N should be chosen depending on the project requirements.

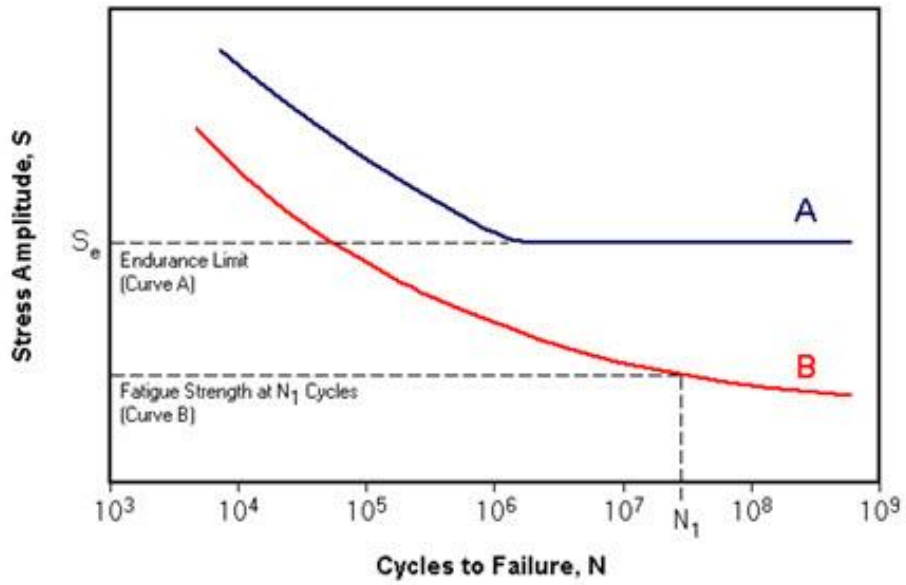

Figure 2.9 - Fatigue endurance limit in different materials [15]

With the studies and experimental tests developed over the years, it was possible to create a correlation, only applicable for steels, between the parameters known about the materials and its fatigue endurance limit, as shown in equation 2.7 [14],

$$S_e' = \begin{cases} 0.504\, S_{ut}\ MPa, & S_{ut} \leq 1460\ MPa \\ 740\ MPa, & S_{ut} > 1460\ MPa \end{cases} \quad (2.7)$$

Where S_{ut} is ultimate stress of the material and S_e' is not the endurance limit of the structure explained before, but the endurance limit of a specimen tested with a quality surface finish, specified size, pure bending load, etc, which has a higher and less conservative value [4]. This value needs to be corrected in order to obtain the real S_e value, with a maximum of six correction factors as equation 2.8 shows [4],

$$S_e = k_a\, k_b\, k_c\, k_d\, k_e\, k_f\, S_e' \quad (2.8)$$

Where k_a is the surface factor, k_b is the size factor, k_c is the loading factor, k_d is the temperature factor, k_e is the reliability factor and k_f is the miscellaneous-effects factor.

2.2.4. Failure criteria

When $\sigma_m = 0$, it is simple to relate the load applied on the component with the S-N curve, because the stress amplitude σ_a corresponds to the fatigue strength in the vertical axis of the S-N curve. When a mean stress σ_m is verified in the cyclic load, the S-N curve alone is not enough and there is the need of a correlation between the mean stress, the stress amplitude and the material properties. Figure 2.10 shows different criteria of failure that were proposed and establish a limit to values that the fatigue load can take.

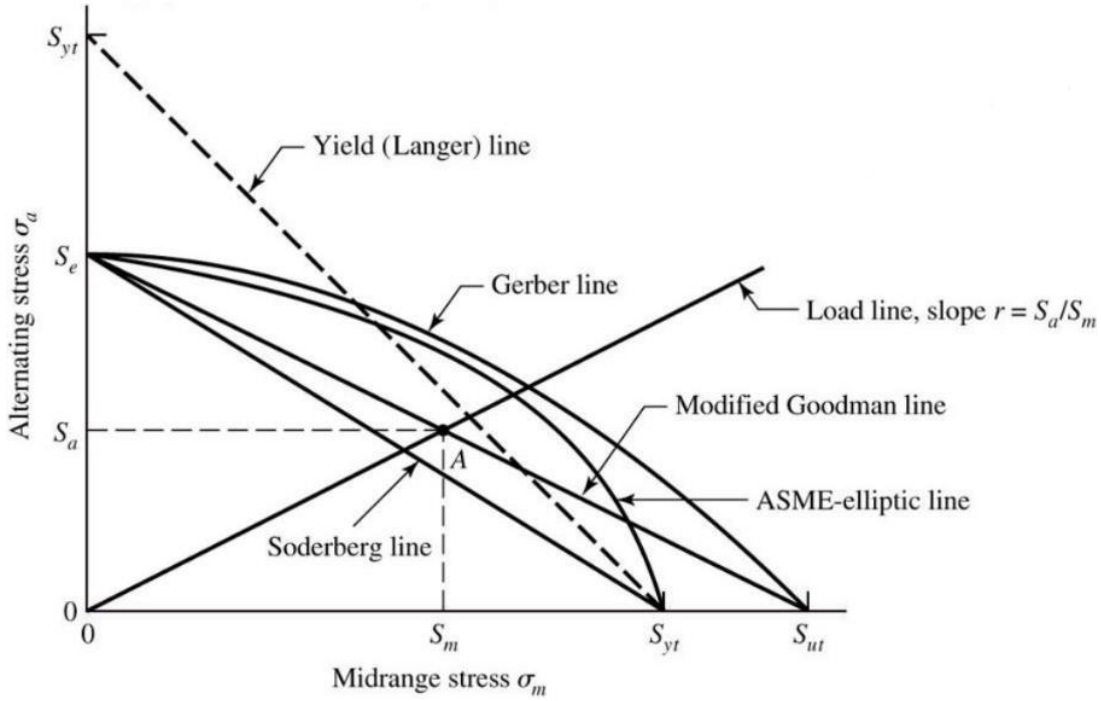

Figure 2.10 - Criteria of failure lines [4]

The modified Goodman line combined with the Yield criteria line provide a tool to verify the result of the fatigue load in the structure and project it for infinite life. Figure 2.11 shows the Goodman-Haigh diagram resulting of this combination.

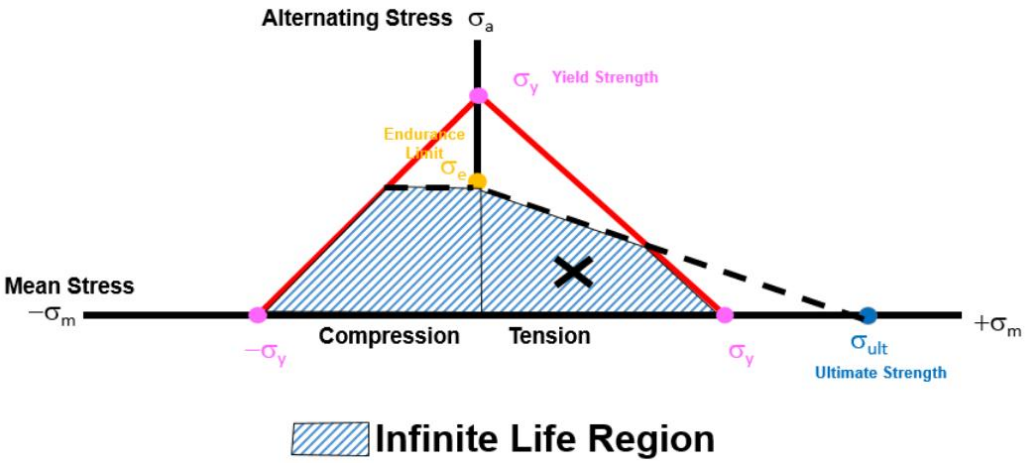

Figure 2.11 - Goodman-Haigh diagram [16]

Equation (2.9) shows the modified Goodman criteria formula [4].

$$\frac{\sigma_a}{S_e} + \frac{\sigma_m}{S_{ut}} = \frac{1}{n} \tag{2.9}$$

Equation (2.10) shows the Yield criteria formula [4].

$$\frac{\sigma_a + \sigma_m}{S_y} = \frac{1}{n} \tag{2.10}$$

In both equations n is the safety factor referring to the infinite fatigue life and when it is equal to 1 means that the point with the coordinates (σ_a; σ_m) in the Goodman-Haigh diagram coincides with the lines that delimit the safe area. For points inside the blue area of the diagram, the components have infinite life with a safety coefficient greater than 1.

2.3. Fatigue in welded joints

For complex welded components, the nominal stress to be compared with the fatigue strength of the material can be difficult to define, even if the stress distribution is very well described with Finite Element Analysis (FEA). Therefore, new improved methods to predict fatigue have been developed. Today there are mainly four methods to predict fatigue on welded components [17]:

- Evaluating the nominal stress
- Evaluating the structural stress
- Evaluating the effective notch stress
- Applying the linear-elastic fracture mechanics

The nominal stress can be calculated in components with low complexity in its geometry and loads, using elementary theories of structural mechanics. Figure 2.12 shows the variation of the nominal stress in a beam-like component, where the effect of the weld is ignored. In more complex geometries the nominal stress can be difficult to determine and distinct S-N curves have to be compiled for a large number of different weld joints.

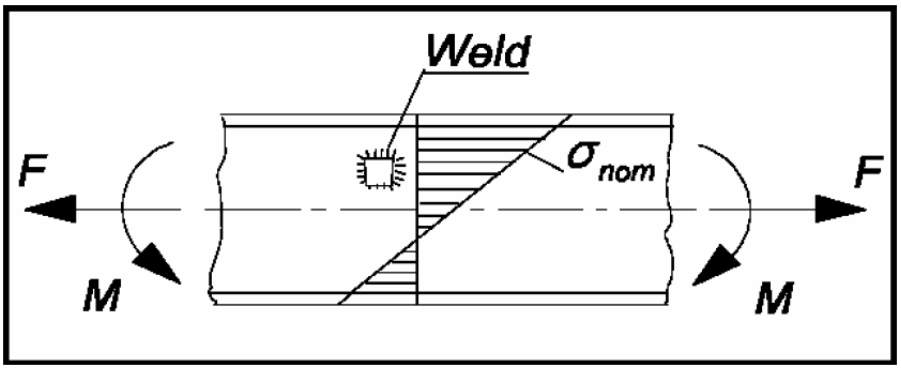

Figure 2.12 - Nominal stress distribution [17]

Each S-N curve is identified by its FAT-value that is the characteristic fatigue strength of the material at 2 million load cycles. Figure 2.13 shows the effect of different structural weld details in the FAT-value and the S-N curve.

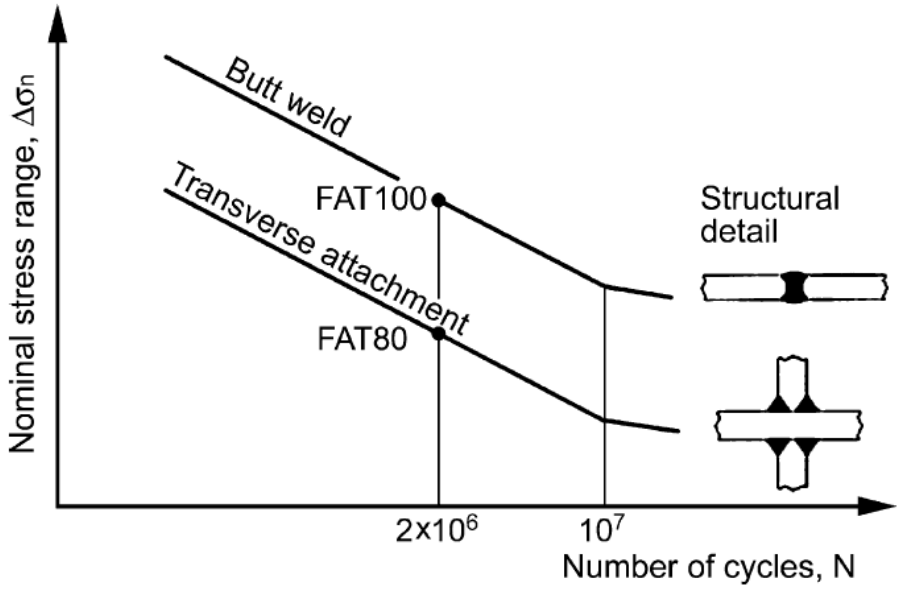

Figure 2.13 - Different FAT classes depending on the structural details [18]

Figure 2.14 shows an example of a welded joint and the corresponding FAT values applicable.

611	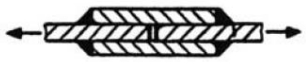	Transverse loaded lap joint with fillet welds Fatigue of parent metal Fatigue of weld throat Stress ratio must be **0<R<1 !**	 63 45

Figure 2.14 - Welded joint 611 and the corresponding FAT values in MPa [17]

Figure 2.15 shows the peak nominal stress that is added to previous stress distributions, when a welded connection is added. The stress remains the same away from the attachment.

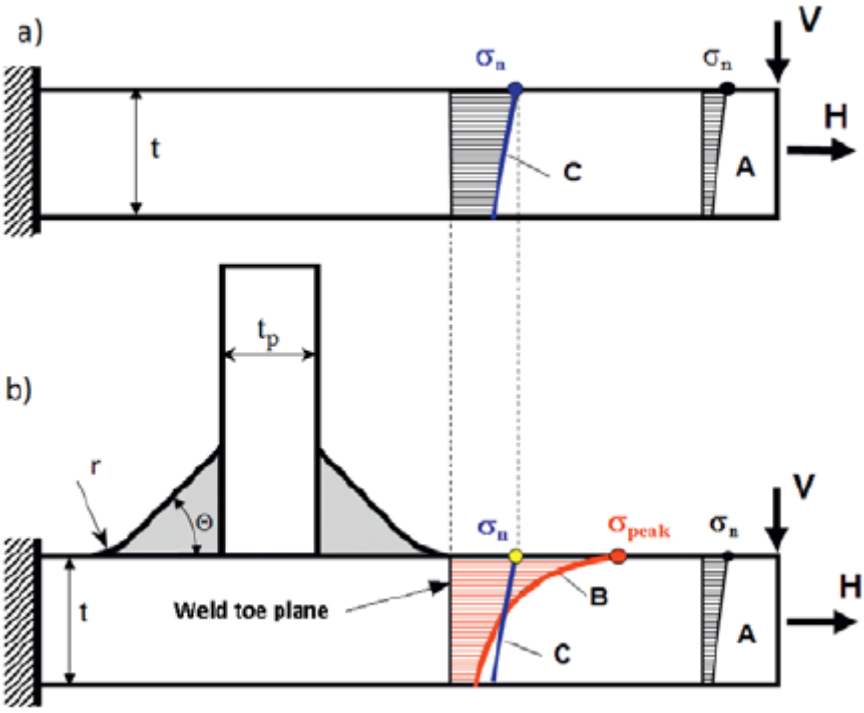

Figure 2.15 - Nominal stress (a) in the base material, (b) with a peak resulting from the attachment [19]

The structural or geometrical stress includes all stress raising effects of a structural detail excluding all stress concentrations due to the local weld profile itself. Figure 2.16 shows the different structural stress distribution resulting from the weld geometries.

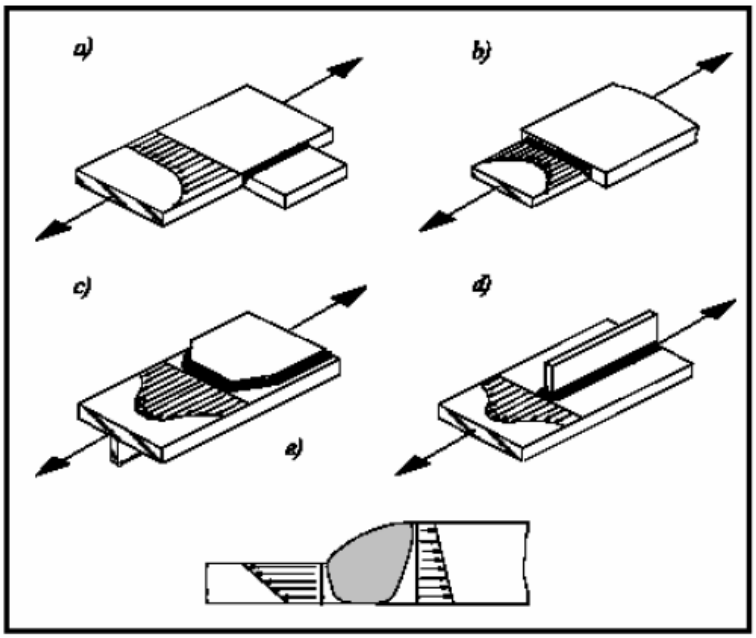

Figure 2.16 - Structural stress of different weld details [17]

This method is mainly used as an alternative when the nominal stress is difficult to define. It is recommended to use the stresses evaluated from FEA at specified distances from the weld toe and then extrapolate them to the weld toe using procedures that will be explained later in the document.

The effective notch stress is the total stress at the root of a notch, obtained assuming linear-elastic behaviour of the material. To take account of the statistical nature and scatter of weld shape parameters, as well as of the non-linear material behaviour at the notch root, the real weld contour is replaced by an effective one. For structural steels an effective notch root radius of r = 1 mm has been verified to give consistent results [17]. Figure 2.17 shows the principle of setting notch radius as 1 mm in all the weld toes and also weld roots, if applicable.

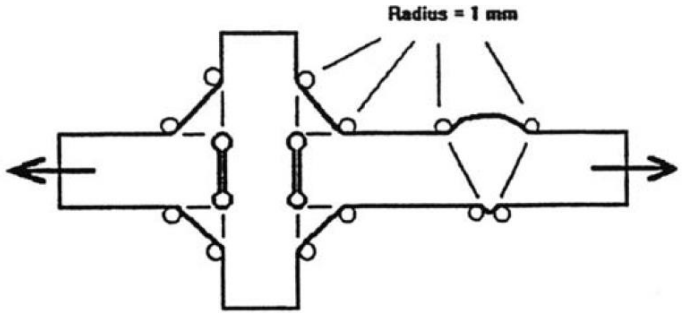

Figure 2.17 - 1 mm radius applied in weld notches [17]

Figure 2.18 shows the difference between 2 structural notches depending on the weld geometry. In the first image the radius of the weld (r_m) is 0,45 mm. In the second image, r_m = 17 mm resulting in a smoother transition from the attachment to the base material and a decrease in the stress concentration value.

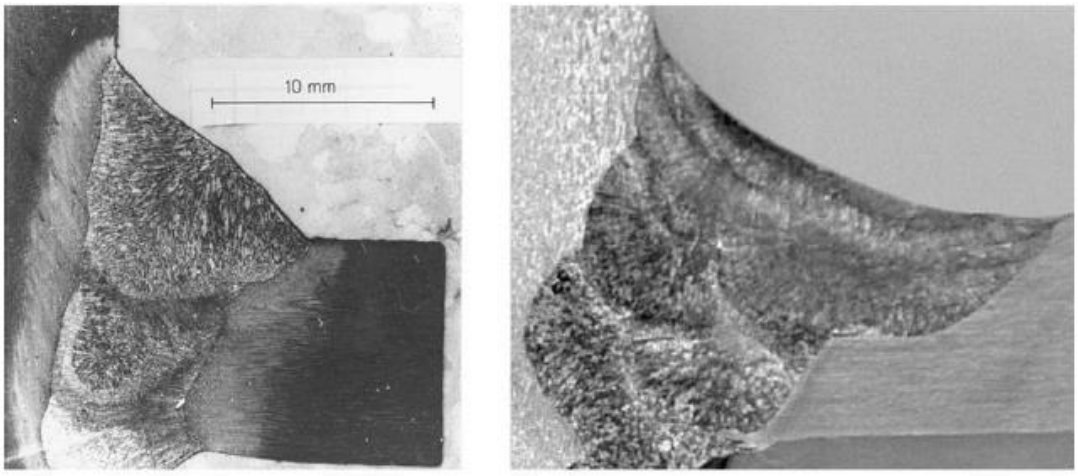

Figure 2.18 - Weld notch comparison [20]

This method is very powerful when a comparison study of different weld geometries and unconventional welded joints is carried out. The effective notch method can handle failure from both toe and root sides but the method is restricted to medium and high-cycle fatigue ($N > 10^5$ cycles). The notch-strain approach should be used for low-cycle fatigue. The method is limited to base material's thickness higher than 5 mm.

The linear-elastic fracture mechanics is used when there are imperfections like flaws, slag intrusions or microcracks resulting from the manufacturing process of the welds. This means that the crack initiation period is only a fraction of the total life of a welded joint and the majority of the life of the components is spent during the crack propagation. In order to estimate the fatigue life, an initial size (a_i) and a final size (a_f) or a critical stress intensity factor (ΔKc) has to be defined. Stress intensity factors can be achieved using handbook solutions, weight functions or numerical solutions. When using weight functions, the stress in the remaining ligament normal to the unbroken assumed crack path is used. This method will save a lot of time compared to a FEA of a crack. To avoid stress singularities at the weld toe and root, they have to be fictitiously rounded according to the effective notch stress theory explained before. This means that if an effective notch stress fatigue assessment is performed, it is easy to perform a fracture mechanics analysis later. Paris law is used to predict life. Weld quality may be introduced into this method by analysing different weld geometries and initial crack sizes based on acceptance limits and postulated design defects.

Table 2.1 summarizes of what is explained in this chapter.

Table 2.1 - Welded joints fatigue assessment approaches [21]

Assessment	Type of a fatigue action	Information
Component test	Load on component	No information
S–N curve of detail	Nominal stress	Structural detail
S–N curve of weld	Structural hot-spot stress	Type of weld
S–N curve of material	Notch stress	Effective notch stress
Paris power law	Stress intensity at cracktip	Material parameters

2.3.1. Hot-spot stress

In the fatigue assessment of welded joints, the weld edges are considered the most critical areas to develop cracks and lead to the components' failure [22]. These areas are characterized by higher stress values compared to its surroundings due to the geometrical discontinuities. This peak value is called the hot-spot stress and consists in the structural stress resulting in the weld toe or weld root, as illustrated in figure 2.19.

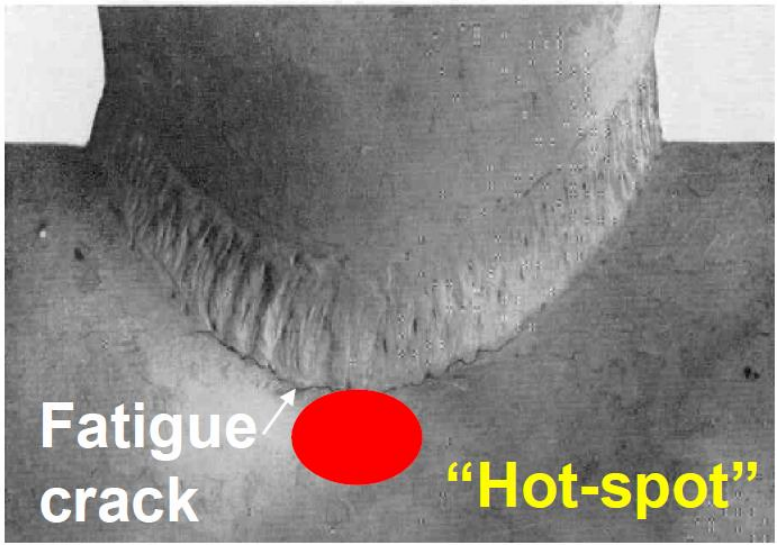

Figure 2.19 - Hot-spot stress location [22]

The hot-spot stress includes all concentrating effects except the local notch effect of the weld toe or weld root introduced by the weld geometry. In the surroundings of the weld the stress distribution is given by 3 components:

- Membrane stress (σ_{mem})
- Bending stress (σ_{ben})
- Non-linear stress peak (σ_{nlp})

These 3 components are illustrated in figure 2.20, with their distribution through the thickness.

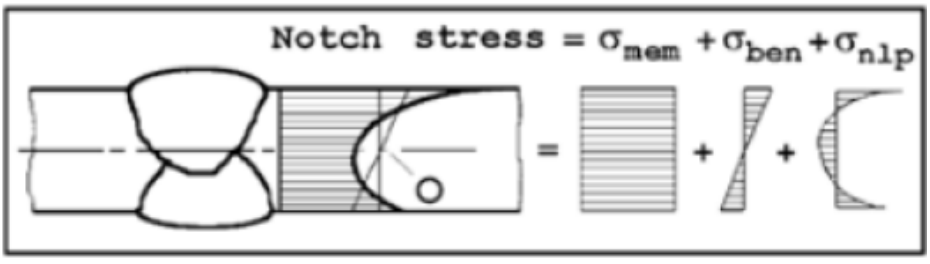

Figure 2.20 - Weld notch stress composition [23]

Where σ_{mem}, σ_{ben}, and σ_{nlp} are given by the equations (2.11), (2.12), (2.13), respectively and t is the thickness of the base material and x is a fraction of that thickness [24]:

$$\sigma_{mem} = \frac{1}{t}\int_{x=0}^{x=t} \sigma(x).\,dx \tag{2.11}$$

$$\sigma_{ben} = \frac{\sigma}{t^2}\int_{x=0}^{x=t} \sigma(x).\left(\frac{t}{2} - x\right).\,dx \tag{2.12}$$

$$\sigma_{nlp} = \sigma(x) - \sigma_{mem} - \left(1 - \frac{x}{2}\right).\sigma_{ben} \tag{2.13}$$

The membrane and bending stress components are associated to the structural geometry. The third component is associated to the weld geometry and is a consequence of the notch effect. The structural stress method intends to exclude this third components from the calculations and include its effects in the S-N curve.

Given this, the hot-spot stress is only a sum of the membrane and bending components. Its difference to the total notch stress is visible in figure 2.21.

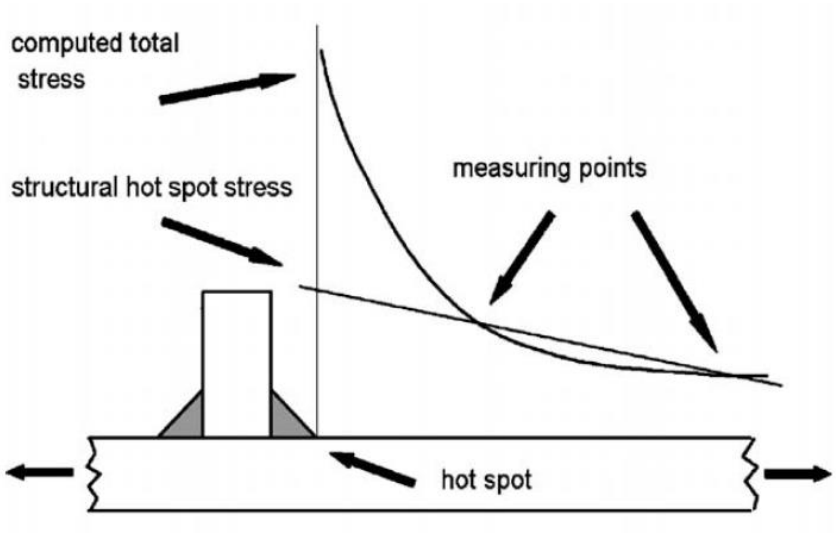

Figure 2.21 - Hot spot stress extrapolation [21]

Some of the advantages of the hot-spot structural stress method are:

- it is applicable to more complex geometries where the nominal stress method can show unsatisfying results;
- less S-N curves are needed for the fatigue assessment;
- it is possible to include a non-catalogued detail in the model.

In figure 2.22 the typical hot-spot stress S-N curve is represented. The fatigue strength parameter in the vertical axis is a stress range resulting from the extrapolation methods that are described later.

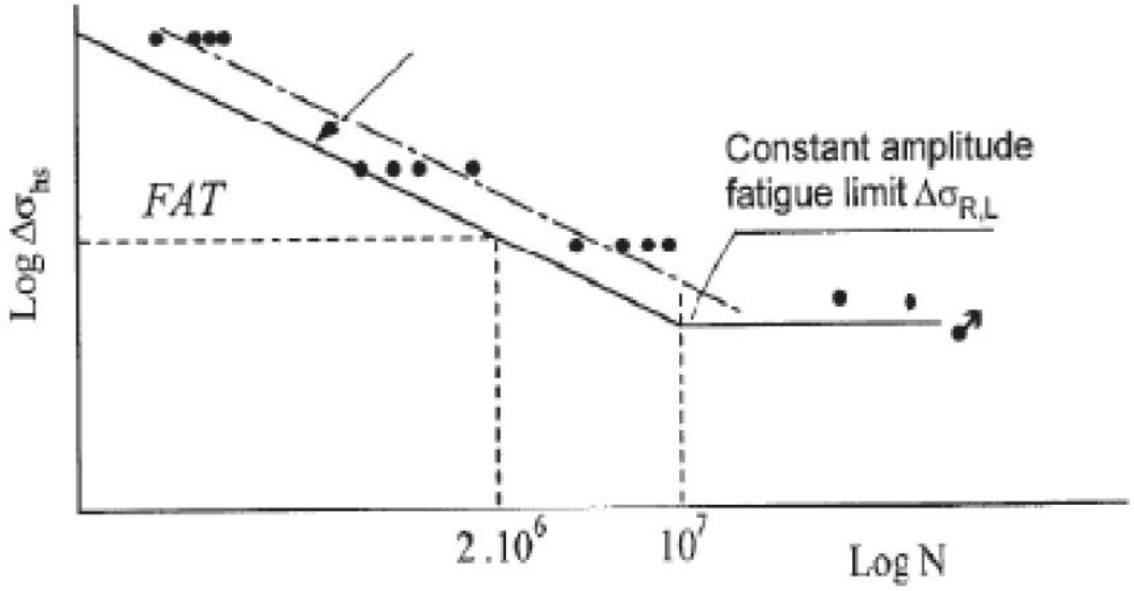

Figure 2.22 - S-N curve for structural hot-spot stresses [25]

Equation (2.14) shows the analytical relation between the stress range and the failure cycles, where C is a parameter of the FAT class used in the fatigue assessment and m is the symmetric of the slope of the graphic. This formula is only applicable for stress ranges that do not show an infinite life.

$$\Delta\sigma_{HS}^{m} . N = C \tag{2.14}$$

2.3.2. Extrapolation methods to obtain hot-spot stresses

The hot-spot stress can be evaluated from two different kind of extrapolation:

- The first option is to perform a linear or quadratic extrapolation (depending on the number of points that are used to obtain the last one) of points at the surface of the base material where the attachment is welded. This is used for hot-spots at the weld toe;
- The second option consists in linearizing the values of the membrane and bending stress in a path along the thickness of the base material. This is used for hot-spots at the weld root.

In total, five extrapolation methods will be explained.

2.3.2.1. Extrapolation on the surface

Figure 2.23 shows an attachment welded to a base plate. It is visible that the weld geometry has a weld toe in the interface with the base material and a weld toe in the interface with the attachment. Type “A” extrapolations are intended to assess the fatigue in the weld toe of the base plate. Type “B” extrapolations are intended to assess the fatigue in the weld toe of the attachment.

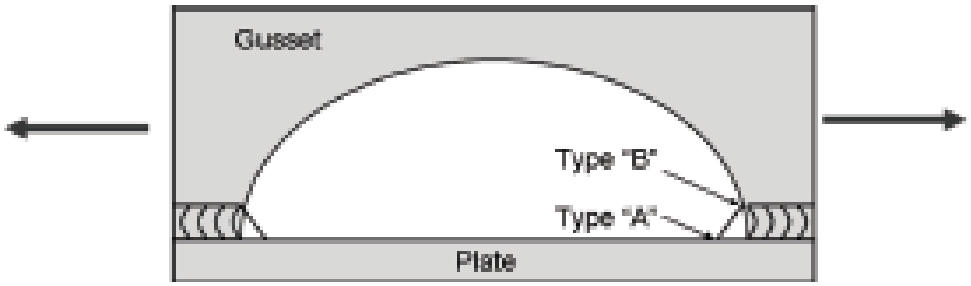

Figure 2.23 - Different types of surface extrapolation [26]

The stress considered all point is a range between the maximum and minimum principal stresses evaluated by the finite element software. Both types “A” and “B” can be applied to finite element models with a fine or coarse mesh. Based on this, there are 4 types of extrapolations that can be performed on the surface [27]:

- Type “A” on a coarse mesh with elements having lengths equal to the plate thickness. This is a linear extrapolation that follows the equation (2.15) and is applied as image 2.24 shows.

$$\sigma_{hs} = 1.5\,\sigma_{0.5t} - 0.5\sigma_{1.5t} \tag{2.15}$$

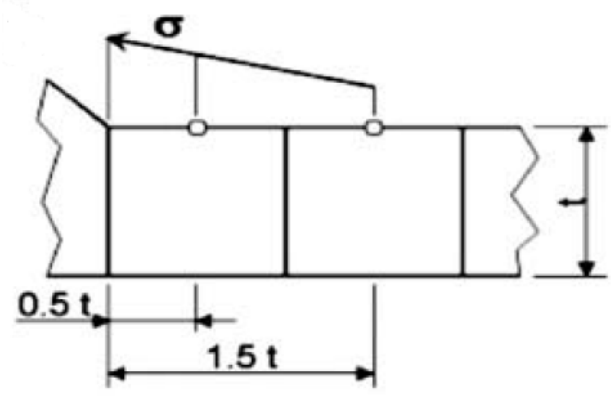

Figure 2.24 - Type “A” extrapolation with a coarse mesh [27]

- Type “A” on a fine mesh with elements lengths smaller than 40% of the plate thickness at the hot-spot. This is a linear extrapolation that follows the equation (2.16) and is applied as image 2.25 shows.

$$\sigma_{hs} = 1.67\ \sigma_{0.4t} - 0.67\sigma_{1.0t} \tag{2.16}$$

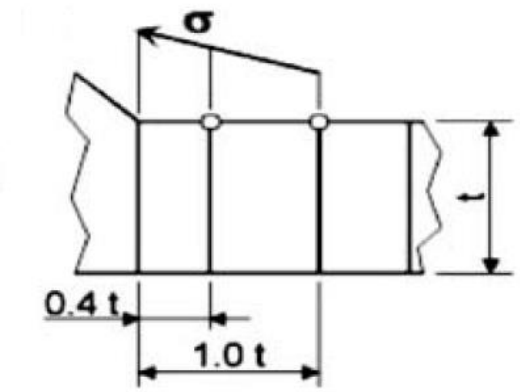

Figure 2.25 - Type “A” extrapolation with a fine mesh [27]

- Type “B” on a coarse mesh with elements having lengths equal to 10 mm at the hot-spot. This is a linear extrapolation that follows the equation (2.17) and is applied as image 2.26 shows.

$$\sigma_{hs} = 1.5\ \sigma_{5mm} - 0.5\sigma_{15mm} \tag{2.17}$$

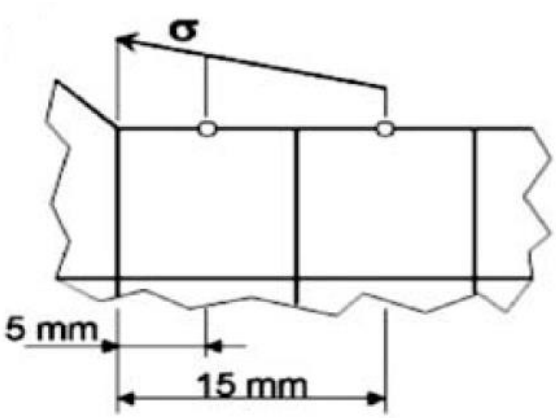

Figure 2.26 - Type “B” extrapolation with a coarse mesh [27]

- Type “B” on a fine mesh with element lengths smaller than 4 mm at the hot-spot. This is a quadratic extrapolation that follows the equation (2.18) and is applied as image 2.27 shows.

$$\sigma_{hs} = 3\,\sigma_{4mm} - 3\sigma_{8mm} + \sigma_{12mm} \tag{2.18}$$

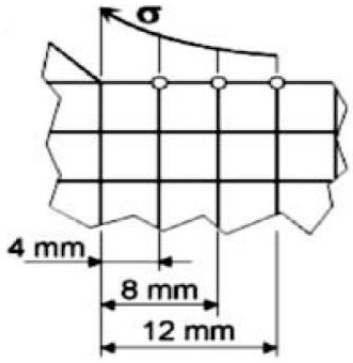

Figure 2.27 - Type “B” extrapolation with a fine mesh [27]

2.3.2.2. Extrapolation through the plate thickness

In this method the stresses evaluated by the finite element software are simply the membrane and bending stresses. The hot-spot stress in the weld root is then given by equation (2.19).

$$\sigma_{hs} = \sigma_{mem} + \sigma_{ben} \tag{2.19}$$

Since the weld root is a hot-spot, due to the geometrical discontinuity, all stress values evaluated at those points are not valid. Figure 2.28 shows the procedure behind the linearization, where a path is created in all the lines that the mesh originated. The linearized sum of the membrane and bending stresses is evaluated in all these nodes of the path and the hot-spot stress is obtained in the last point.

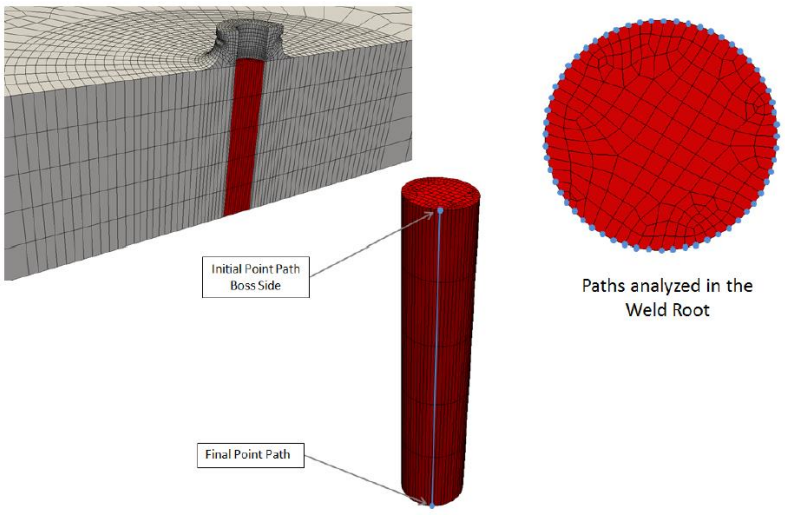

Figure 2.28 - Stress linearization through thickness [28]

3 Case Study

3.1. ITER PPR Project

International Thermonuclear Experimental Reactor (ITER) is an organization based in France and composed by 35 nations from all over the world that is developing an ambitious nuclear fusion energy project, by designing the biggest Tokamak of the world.

The Tokamak is an experimental machine designed to harness the energy of fusion. Inside a tokamak, the energy produced through the fusion of atoms is absorbed as heat in the walls of the vessel. Just like a conventional power plant, a fusion power plant will use this heat to produce steam and then electricity by way of turbines and generators.

The ITER Plasma Position Reflectometry (PPR) system is part of the magnetic diagnostic systems and measures the density profile of the plasma circulating inside the Vacuum Vessel (VV). This provides real-time measurement of the distance between the plasma and the VV wall among other parameters.

3.2. Problem description

Some of the PPR system components need to be attached to the VV wall. The solution used for this attachment was to weld bosses in the wall and screw the components to this boss. As the measure components, the bosses and their welded connections will be exposed to large amounts of heat and electromagnetic forces, despite the presence of protective blankets installed [29].

Given this problem, a fatigue assessment is required in all the welded connections located inside the VV and this work will focus in the support of an antenna in one of the blanket gaps.

Thermal and structural analyses will be conducted using the finite element software Ansys® and based on the results, the geometry will be modified to comply with ITER's requirements.

This work was divided in 3 main steps:

-Identify which would be the worst load case scenario among 7 that are applied to the geometry and will be explained later.

-Calculate the safety factory in terms of fatigue failure in the 2 most demanded areas of the weld (weld root and weld toe), using the worst load case, chosen before. This evaluation considers the resulting stresses on the model and the duration of the load (the number of times it is cyclically repeated). The geometry was changed 2 times and this step was repeated to check for the improvements.

-Calculate the total fatigue safety factor of the project using the third geometry where the resulting stresses are lower. This was done for each load case given and in the most critical point of the weld.

3.3. Initial geometry

The pressure vessel structure has a circular shape and is where the plasma formed will circulate. It is illustrated in a cut view in the figure 3.1.

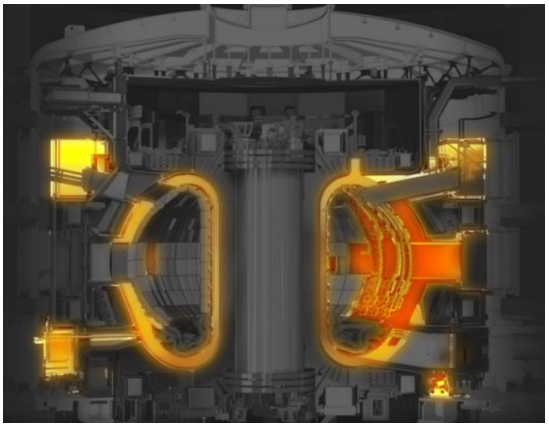

Figure 3.1 - ITER Pressure vessel [29]

A section of the VV (developed and studied previously by ITER, to get the loads and boundary conditions to applied in this study) is shown in figure 3.2 (a) and in figure 3.2 (b) it's represented the geometry that will be used in the fatigue assessment, which is a sub-model of the full VV body.

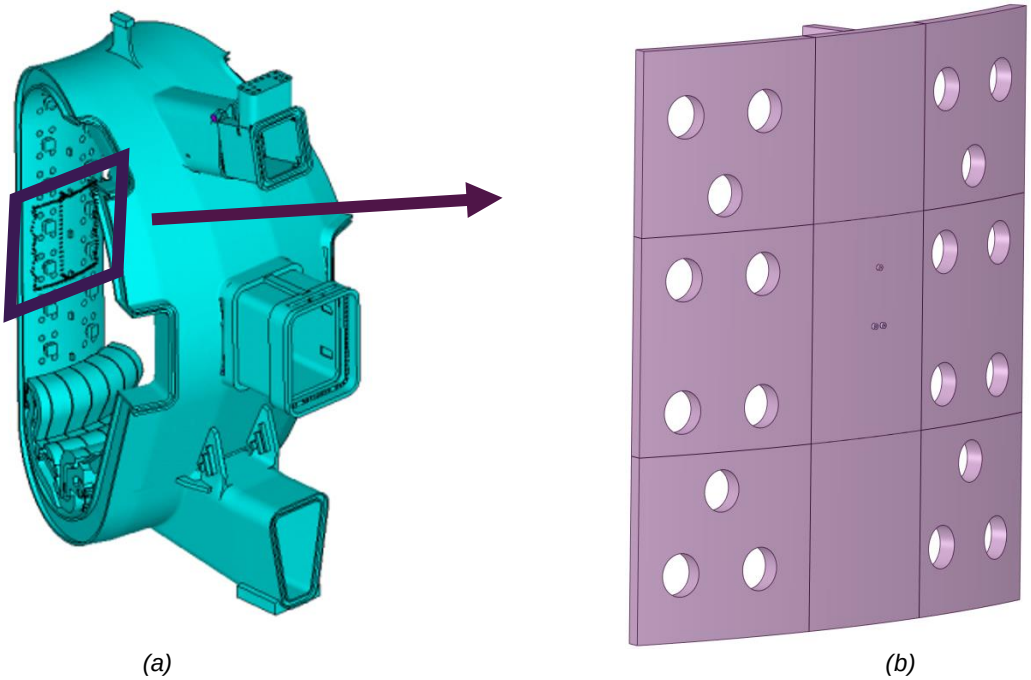

(a) *(b)*

Figure 3.2 - a) Circular section cut of the VV [28]*, (b) sub-model geometry*

The minimum number of bosses necessary to support the weight of the antenna was settled as 3. Based on this, an initial configuration for the bosses was proposed as can be seen in figure 3.2 (b). The bosses' arrangement can be changed, as long as the support's center keeps in the same place, because that is where the blanket gap is and where the antenna tip will have to be located.

3.4. Load scenarios

There are 5 load cases, defined by ITER, that can be applied on the model and each of them will be repeated a certain number of times during the time that the Tokamak will operate. Here is a description of these phases:

-The plasma formation consists in creating the material that will spin inside the VV and release the heat used to produce energy. The machine needs to be designed to take 2591 plasma formation events.

-The normal operation phase consists in the machine working stationary and producing energy. The number of normal operation events was established as 300.

-The baking process is an intermediate maintenance phase when the machine gets ready for the next operation. The number of baking events was established as 500.

-The plasma disruption consists on the plasma inside the VV stopping its spinning motion and applying inertial forces in all the structure. The plasma disruption will occur 3850 times.

-The seismic event represents what would happen to the structure during an earthquake. The number of seismic events considered is 350.

4 Computational numerical methodology

This chapter of the thesis consists on a summary of the procedures carried out in the software Ansys® and Matlab®. The first one uses the finite elements method to solve mechanical problems and Matlab is used to rearrange information used as an input in Ansys. The different steps required to perform each analysis will be shown in detail.

4.1. Finite element model

Regardless of the software chosen, a finite element model consists in a well-defined geometry, a mesh created on all its parts, boundary conditions that can completely fix the geometry in space or just constraint the movement in certain directions and the loads that will cause it to deform or heat.

In order to obtain valid results a quality mesh has to be generated, so different mesh convergences were performed for every different geometry studied and for each approximation method, as will be described.

4.2. Software used

4.2.1. Ansys

All the analyses were performed with the finite element software Ansys® because it is the one used in ITER, so the communication and the results comparison is easier.

This software has 2 different strands for numerical simulation that are APDL and Workbench. The first one was the original Ansys interface and has some advantages like the parametrization of project values, so it is very versatile for users that know it well. Ansys Workbench has a more user-friendly interface that includes new tools for mesh control and optimization of design points, for example and allows to have a project with several analysis with the different geometries and setups and import the results or material properties between them.

The simulation follows 3 different steps in both options:

-pre-processing, where the geometry is created, imported or changed, the material properties, loads and constraints are defined and the mesh is created;

-solution, where the analysis type is chosen and the mathematical created is solved;

-post-processing, where it is possible to ask for the stress distributions desired and compare and export the values in the form of tables or graphics.

All the geometrical changes and simplifications were made in SpaceClaim, that is a CAD software inside Ansys. This tool is directly connected to Workbench, so there is no need to export, change and then import the geometry file. The results are checked in real time.

4.2.2. Matlab

Matlab is a software intended for numerical calculation and database manipulation. It was chosen because is simple to work with and available in the University.

It was used to get the input information organized and ready to apply in the model. All the data was originally divided in two complementary files and out of numerical order. With the help of this software, it was possible to gather everything in the desired format and file type required by Ansys Workbench.

The scripts written in both cases are attached in the end of the document.

4.2.2.1. Displacement files organization

One of the text files received had the ID number and the coordinate in the 3 main directions for every node belonging to the sub-model boundary. There was also a .cbdo file with boundary nodes ID number and the displacement in the 3 main directions for every load case introduces before.

First, all the .txt and .cbdo files were converted to .csv which is the file format that Matlab can ready. Than all the nodes IDs were organized in numerical order just to make it easier to check the results and the location information was associated to displacement values for each node. The 38644 boundary nodes information was then organized but written in a long text, so it was converted back to a text file with paragraphs, resulting in a line for each node information. The lines were composed by 7 values: node ID; X position; Y position; Z position; X displacement; Y displacement; Z displacement and this info is imported to Ansys has a table.

4.2.2.2 Temperature file organization

The procedure to organize this setup information was the same as with the displacement files but in this case there was only one input file, since the plasma formation is the only load case where the temperatures differs along the geometry. The .txt file had the ID number and the coordinate in the 3 main direction for all the volume nodes and the .bfin file had the ID number and the temperature value.

The resulting text file lines were composed by 4 values: node ID; X position; Y position; Z position; temperature value.

4.3. Steps

The fatigue assessment will be carried out in three different geometries that have different boss arrangements. The first geometry was provided by ITER. The two other geometries have a modification that intends to reduce the stress values at the welds.

4.3.1. Geometry 1

The initial geometry that was presented in chapter 3 was adapted to facilitate the procedures of the analysis. The purpose was to help in the mesh creation and refinement or to facilitate stress evaluations along the thickness, for example.

It is a sub-model of the big VV body as mentioned before but is still a large and complex geometry. The areas farthest from the bosses, seen in figure 4.1 (a) are essential to import all the displacements that will deform the geometry but will not be changed in the geometry optimization, so only the center part in figure 4.1 (b) will be considered in this sub-chapter, to have more detail on the essential body parts.

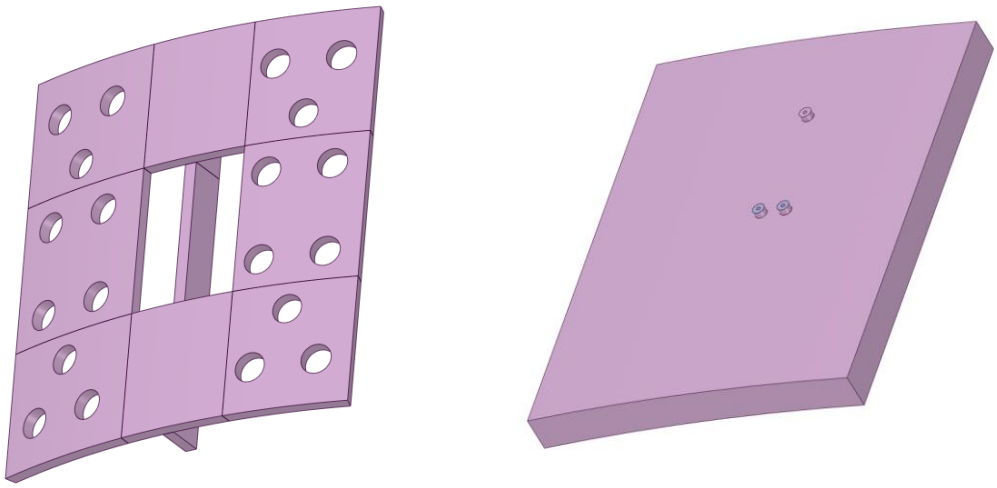

(a) *(b)*

Figure 0.1 - (a) Outer geometry (b) Center of VV

Figure 4.2 (a) shows 2 bodies created with the already existing material around the bosses' area. This allows to create a mesh with different element size, as will be shown later in the mesh convergence step. Figure 4.2 (b) shows 3 bodies created in the VV geometry with the diameter of the bosses and aligned with them and figure 4.2 (c) shows 3 bodies created in the boss wholes alignment. The purpose is to facilitate setting different element sizes for these parts and evaluate stresses in their surfaces.

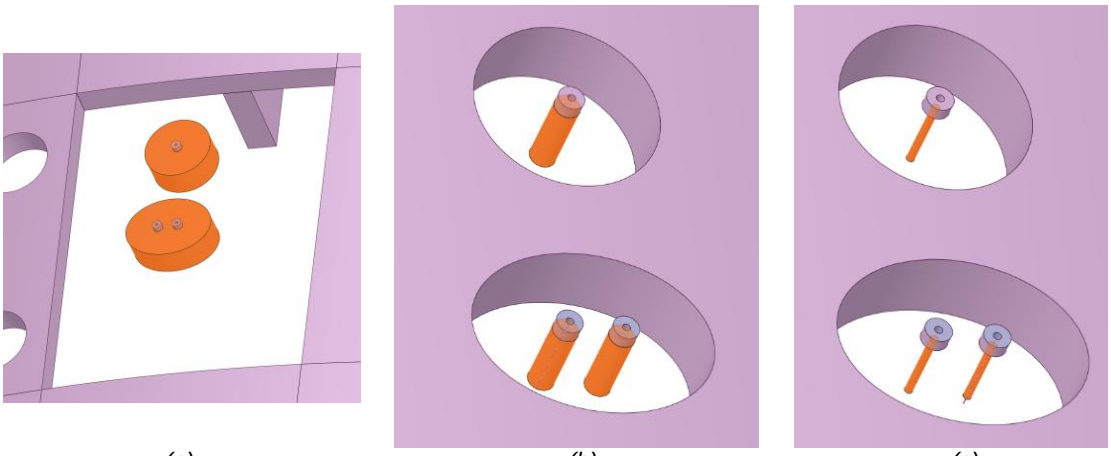

(a) (b) (c)

Figure 0.2 - a) Area around the bosses, (b) Projected area of bosses, (c) Projected area of boss holes

All the bosses used to support the antenna have the same shape and size. In figure 4.3 the boss is represented in blue with its dimensions. The weld geometry can be seen in orange. It is a full penetration weld, so it occupies and strengthens all the contact between the boss and the VV parent material. The point with the number 1 represents the weld root and the point with the number 2 represents the weld toe, the 2 main areas that will be considered in the fatigue assessment.

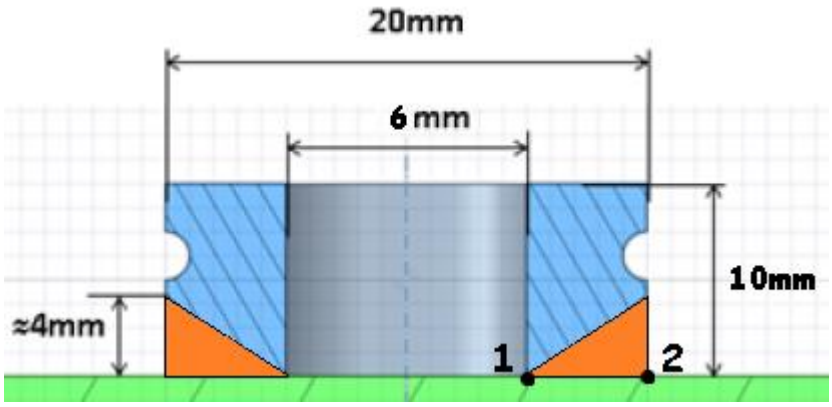

Figure 0.3 - Boss dimensions [28]

The geometry was simplified and the weld toe location coincides with the outer radius of the boss, instead of having a curvature shape from the boss represented in blue to the VV represented in green. This will lead to a higher hot-spot stress in the weld toe because of the geometrical discontinuity.

When trying to find a better geometry, parts of the VV that belong to the sub-modelling boundaries cannot be changed or supressed because the displacements (or a portion of them) would be imported to an area that no longer exists and the operation fails.

4.3.2 Geometry 2

By evaluating the von-Mises equivalent stress in the VV center body of the initial geometry where the bosses are welded, it is visible in figure 4.4 that the 2 bottom bosses are in an area with high stress region on the surface. It they are positioned further away from the top boss, the weld that attaches them to the VV is subject to smaller stresses.

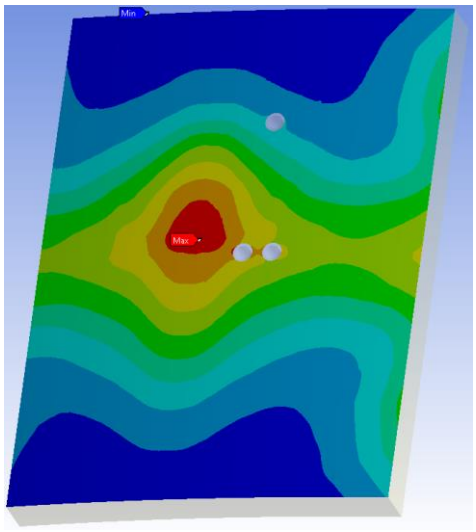

Figure 0.4 - von-Mises stress distribution at surface of geometry 1

The first geometrical change is only increasing the initial distance (L_0) between the top boss center and the 2 bottom bosses center by 40 mm (ΔL), just by moving the bottom bosses down, to check the effect in their weld fatigue life. This distance is now 241 mm and figure 4.5 shows the new bosses' arrangement. It is also noticed that the geometries introduced in figure 4.2 were created again for the same purposes.

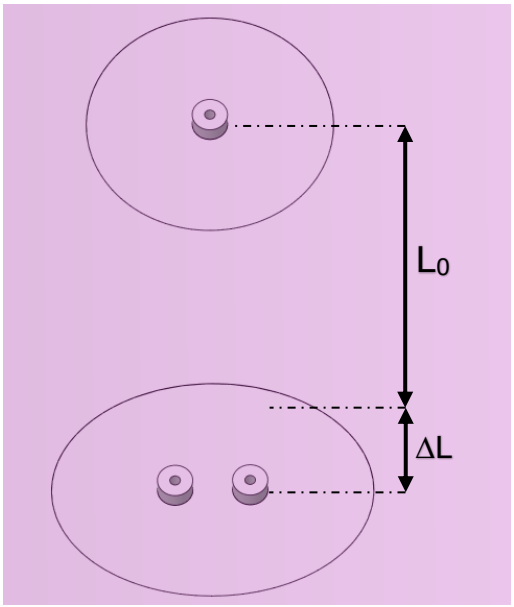

Figure 0.5 - Geometry 2 changes

4.3.3. Geometry 3

The second geometrical change had the geometry 2 as base and consists in increasing the initial distance (L_0) between the 2 bottom bosses center by 47.5 mm (ΔL), just by moving the bottom right boss to the right, to check how the weld toe and root hot-spot stress get affected. This distance is now 90 mm and figure 4.6 shows the new bosses' arrangement. It is also noticed that the geometries introduced in figure 4.2 were created again for the same purposes.

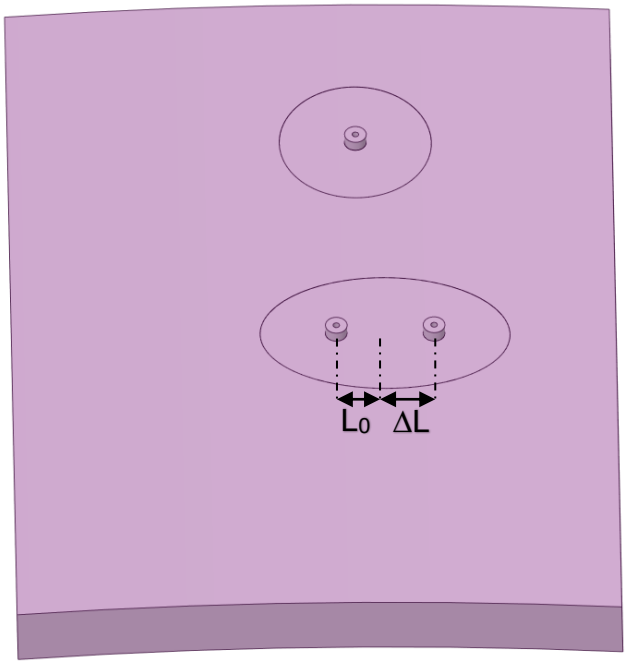

Figure 0.6 - Geometry 3 changes

4.3.4. Material

The material used for the fatigue assessment is the austenitic stainless-steel type 316L (N)-IG. It is the same in all the geometry parts including the bosses and the welding added material, as a simplification.

The default temperature for the model was set to 20 ºC and the material properties vary with the temperature, as can be seen in table 4.1 and was considered in the analysis setup. For each temperature value, the respective value of density (ρ), coefficient of thermal expansion (α), Young's Modulus (E), thermal conductivity (K) and specific heat (C_p) is presented. All the data introduced in Ansys is in SI units.

Table 0.1 - Material properties

T [K]	ρ [kg/m^3]	α [K^{-1}]	E [GPa]	K [W/m.K]	C_p [J/Kg.K]
293.15	7966	1.59E-05	200	13.9	470
323.15	7949	---	---	14.4	476
373.15	7932	1.64E-05	193	15.1	486
423.15	7910	---	---	15.8	497
473.15	7889	1.7E-05	185	16.5	508
523.15	7867	---	---	17.2	518
573.15	7846	1.75E-05	176	17.9	529
623.15	7824	---	---	18.7	539
673.15	7803	1.79E-05	168	19.4	550
723.15	7781	---	---	20.1	560
773.15	7760	1.83E-05	159	20.8	571
823.15	7739	---	---	21.5	582
873.15	7717	1.87E-05	151	22.3	592
923.15	7696	---	---	23	603
973.15	7674	1.9E-05	142	23.7	613
1073.15	7624	---	---	25.1	634
1173.15	7573	---	---	26.6	655
1273.15	7516	1.98E-05	100	28	676
1373.15	7467	---	---	29.4	698
1473.15	7412	2.11E-05	60	30.9	722
1573.15	7355	v	---	32.3	740
1673.15	7297	2.35E-05	19	33.7	761
1873.15	---	2.6E-05	2	---	---

The Poisson's Ratio is equal to 0.3 at any temperature value. At the default temperature of 293.15 K the yield strength is equal to 2.2E8 MPa and the ultimate strength is equal to 5.25 MPa and at higher temperatures these limit strength values are lower. This information is not inserted in Ansys has an input, but the peak equivalent stresses always must be checked to ensure that the material does not deform plastically.

This material was proposed by ITER and is not a variable that will be changed as an initial solution, if the project requirements are not met. In this study only, geometrical changes will be studied to improve the model.

4.3.5. Loads and Boundary Conditions

The normal operation and the baking load case scenarios mentioned before are divided in 2 strands: the thermal and the pressure components. That sums 7 different setups to analyse, instead of 5.

These load cases to be applied on the model consist on displacements applied by node provided in external files combined with a body temperature higher than the default, a pressure or an acceleration.

The displacements values for each principal direction are applied to the model boundary surfaces represented in red in figure 4.7. Workbench reads the text file as a table and the instructions about the order of the values in each line and what they refer to was done in every analysis setup.

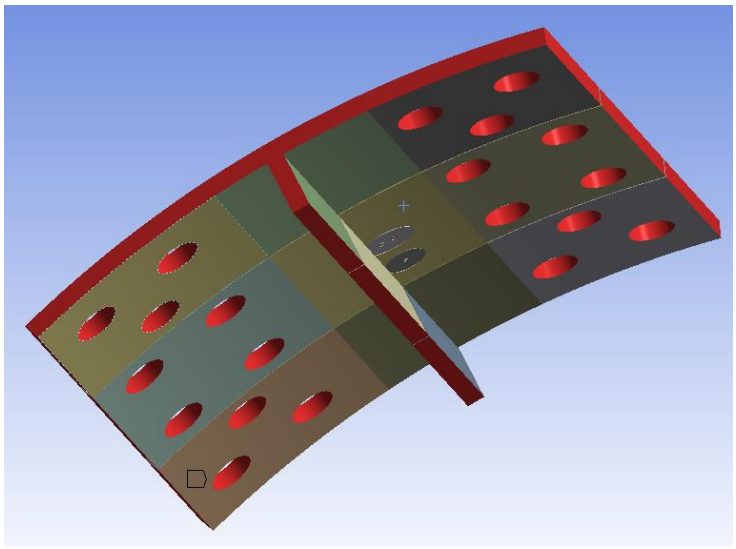

Figure 0.7 - Sub-model boundary faces

Such as in any other structural analysis, there is the need to establish boundary conditions that prevent the body from moving freely and so make it possible to run the simulation. This is also imposed by the displacements imported, as the exact position where each node will be after the geometry gets deformed is being defined. In the thermal analysis performed, there is no movement or load imposed to the body, so the only initial condition set is the reference temperature of 20ºC.

4.3.5.1. Normal operating temperature

In this case, the displacements input is combined with a uniform temperature of 100 ºC in all the geometry parts. The displacements applied to the boundary surfaces can be seen in figure 4.8 and in the next 6 load cases the procedure is similar.

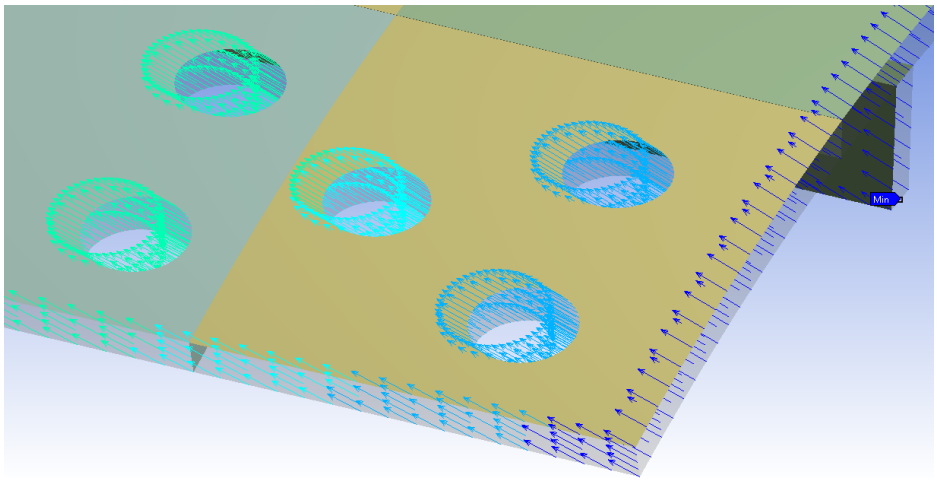

Figure 0.8 - Displacements imposed on the boundary surfaces

4.3.5.2. Normal operation pressure

In this case, the displacements input is combined with a constant pressure of 1.15 MPa in all the outer surface of the VV, which is equivalent to a negative of vacuum pressure inside the VV. Figure 4.9 shows the surface where the pressure will be applied.

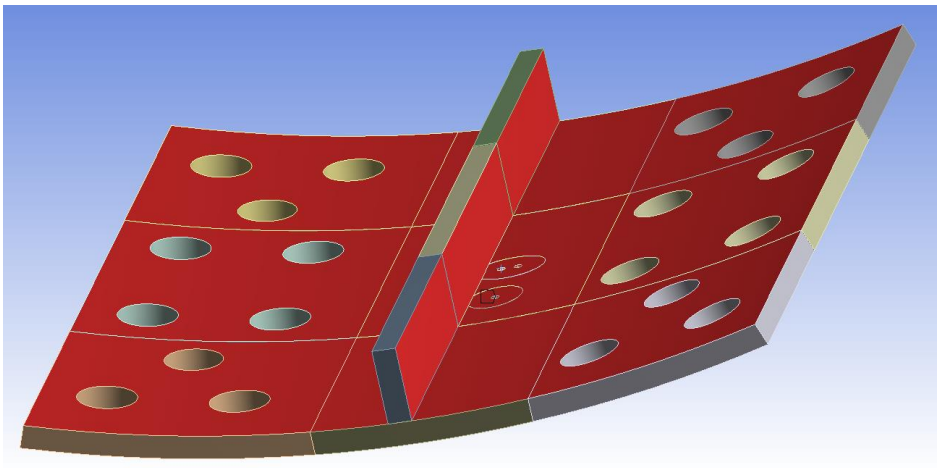

Figure 0.9 - Outer surface

4.3.5.3. Baking temperature

In this case, the displacements input is combined with a uniform temperature of 200 ºC in all the geometry.

4.3.5.4. Baking pressure

In this case, the displacements input is combined with a constant pressure of 2.65 MPa in all the outer surface of the VV represented in red in figure 4.9, which is equivalent to a negative of vacuum pressure inside the VV.

4.3.5.5. Plasma formation

In this case, the displacements input is combined with a temperature that has different values all along the geometry and varies between 100 to 191 ºC. This input was also provided in an external file and its applied on each node of the whole volume mesh (not just in the boundary surfaces). The temperature distribution in the geometry is visible in figure 4.10.

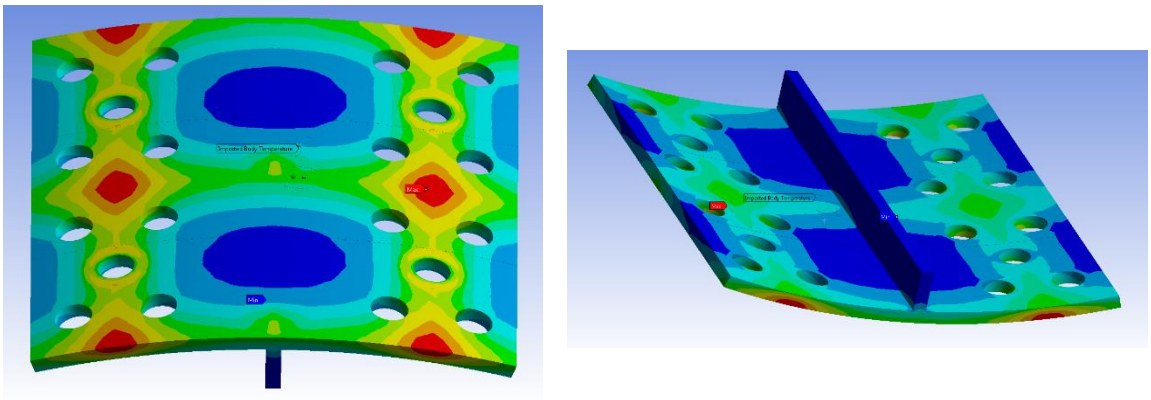

(a) *(b)*

Figure 0.10 - Plasma temperature distribution (a) inside the VV, (b) outside the VV

4.3.5.6 Plasma disruption

In this case, the displacements input is combined with a constant pressure of 899 KPa in all the inner surface of the VV. This is physically the opposite of what happens in the normal operation and the baking phases, as it is a positive pressure inside the VV chamber. The surfaces where the pressure is applied are shown in figure 4.11.

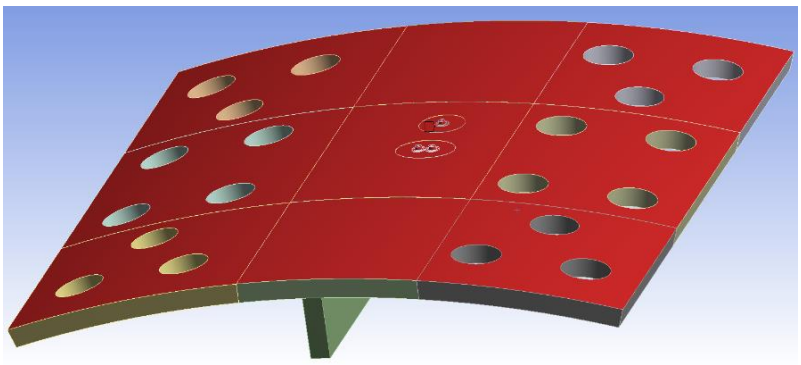

Figure 0.11 - Inner surface

4.3.5.7. Seismic event

In this case, the displacements input is combined with an acceleration applied in all the geometry. The effect in the model is similarly to the gravity acceleration, but with a slightly smaller value and not in the vertical direction.

4.3.6. Element selection

Ansys has a diversified element library with distinct types that can be applied to type of analysis performed (structural, thermal, fluid, …). The element type can be chosen by the software or by the user, if there is the need to comply with some requirement. In the present study this parameter was always selected automatically by the software, despite it was given the instruction to prefer hexahedral elements.

The elements of the mesh can be solid, shell if the thickness of the bodies is not defined or solid-shell which is an intermediate case used for example to evaluate certain type of stresses.

Most of the analysis performed were steady-state structural and the model always has a well-defined thickness in all the volume, so the elements used (automatically defined by Ansys) were SOLID186 and SOLID187.

The steady-state thermal analysis performed used the same geometry, so the model also had a well-defined thickness in all the volume and the elements used by the software were SOLID87 and SOLID90.

All the element types used are tri-dimensional and have a characteristic of reduced integration which makes the analysis run faster keeping precise results. SOLID90 and SOLID186 have a hexahedral quadratic structure with 20 nodes. SOLID87 and SOLID187 have a tetrahedral quadratic structure with 10 nodes, as is represented in figure 4.12.

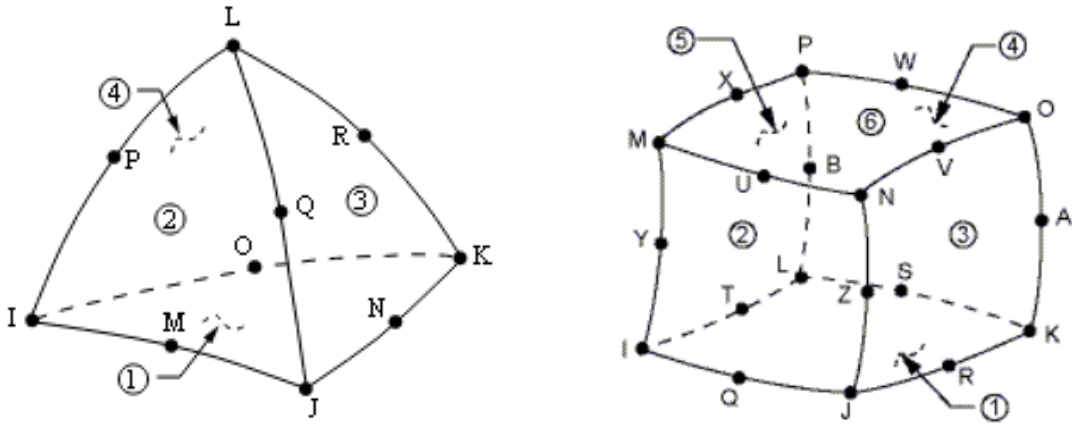

(a) *(b)*

Figure 0.12 - (a) Tetrahedral mesh element [30], (b) Hexahedral mesh element [30]

4.3.7. Mesh

The mesh applied on the model is one of the most important parameters to consider when setting up the analysis because it will be the base of the mathematical calculations performed by the finite element software. Before running an analysis with valid results, a mesh convergence study needs to be performed. This process consists in finding the maximum element size that ensures accurate results. If the element size applied is too big and the mesh has not yet converged, the results obtained can change a lot every time the analysis runs. This can be performed in all the model, but usually is done in the volume, area, edge or point of interest where the results will be assessed, to minimize the number of nodes and elements in the model. The remaining part of the model should just have a relatively fine mesh. That is also the reason to choose the biggest element size that started to produce converged results.

Given this, it is preferable to have a mesh with too small elements that will take more time to run an analysis than to have a coarse mesh that will produce wrong results, but the ideal is to have the minimum element number that ensures all the conditions stated before, so that the model is the lightest possible.

For each element size chosen during the mesh convergence, the result value evaluated should be the maximum von-Mises stress, the maximum total deformation or the maximum temperature, once it is the one that varies the most. Stress values are harder to converge that deformations, so that was the parameter used in all the convergences of structural analysis

In this specific case, before the convergence of the results it must be ensured that the boundary surface had enough nodes to import all the displacements. Ansys Workbench applies the source data in any mesh but if a poor mesh is used, the software will have to extrapolate the deformation value in the areas without any corresponding input value and part of the information is lost, also affecting the results. All the displacement text files have information for 38644 nodes and using 10 mm elements in the outer bodies of the VV results in 40415 target nodes, so all the data is imported successfully. In the thermal analysis performed for the plasma formation load case is applied the same principle but referring to the whole geometry and not just to the sub-model boundaries. The input file has a temperature value for 1331990 nodes and the resulting mesh should have more nodes.

In figure 4.13 is possible to see the refinement difference between the center of the geometry where the bosses are and where the approximation methods will be applied and the surroundings.

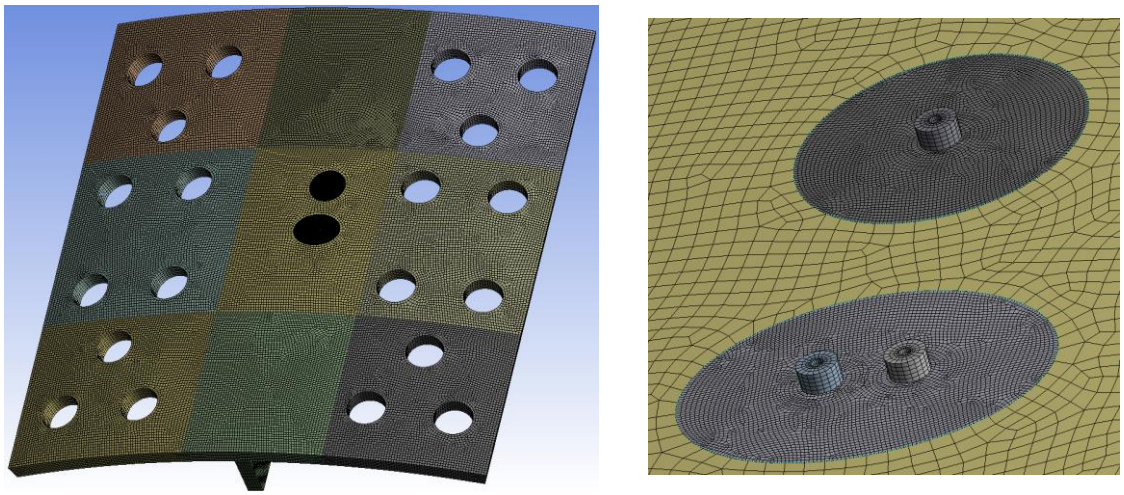

(a) (b)

Figure 0.13 - Mesh (a) in all the geometry, (b) contrast in the interest zones

4.4. Analysis

In this chapter the procedures for each analysis developed are explained. In some of them the steps are the same and only the setup is changed, so only one mesh convergence is required. In others cases the inputs are constant and the geometry changes and/or is used another extrapolation method to obtain the hot-spot stress, so the mesh convergence needs to be done again for the new conditions.

The first 7 analyses were performed using the initial geometry to determine which load case would create more stresses in the VV. Then 2 analyses were performed to calculate the fatigue safety factor in the weld root and in the weld toe. This step was repeated for the two new geometries created and with the last geometry it was possible to apply another extrapolation method of the hot-spot stress due to the new distance between the bosses. The last 3 analyses used the third geometry and the worst load case scenario to estimate the total fatigue safety factor for the welded connections.

4.4.1. Mesh Technique

Following the requirements for mesh creation mentioned before, 4 different types of mesh were created. Each type was converged on distinct geometry points but all have these initial steps in common:

-Attribute a meshing method to all parts of the geometry and choose if the element type will preferably hexahedral or tetrahedral. It is preferable to have elements with square triangular faces.

-Set the property ‘Share Topology’ to ‘None’ and the property ‘Merge Nodes’ to ‘Disabled’. Following this, the number of nodes in the interface of two bodies can differ and so they will not coincide in these two surfaces but it prevents from occurring errors generating the mesh or ending up with a large number of tetrahedral elements.

-The element size at each part can be defined using and edge sizing, face sizing or body sizing. This instruction is combined with the meshing method chosen to achieve a uniform shape in the mesh and to avoid having an abrupt change in size between two parts that touch each other or inside a part with a cylindrical shape for example.

-10 mm dimension was attributed to the elements in VV areas that will not change and where any extrapolation method will be carried out.

-6 mm size was attributed to the 2 bodies around the bosses. These 2 body parts will be the target of the mesh convergence in some cases, so they will change. In the cases when its kept, it creates a relatively fine mesh, resulting in a soft element size transition to the bosses.

-The element size of the bosses attached to the Vessel was set to 2 mm. This creates a heavy mesh in this three bodies but will not affect much the model because they have a relatively small volume. Those are parts of the geometry where stresses and deformations will not be evaluated but are in direct contact with the relevant areas where the mesh convergence will be made.

4.4.2. Determine the worst load case scenario

In this analysis group the initial geometry was used with all the adaptations shown in chapter (4.3.1) and the mesh creation only followed the steps in chapter (4.4.1). This case does not require a more refined mesh in any areas because despite the area around the bosses is the one in concern, the results were compared all over the geometry.

With this common base, 7 analyses were created, each using one of the 7 load cases described before as setup. The von-Mises equivalent stress was the output used for comparison.

The importation of the external data files is described in the following steps:

1) Associate the text file to the analysis setup;
2) Attribute a name to the file;
3) Identify the content inside the file (node ID, node coordinates, displacement values or temperature value);
4) Attribute a name to the displacements in X, Y and Z or to the temperature value;

5) Create a displacement or temperature import inside the analysis;

6) Associate the name chosen in step 4 with the displacement component inside the analysis.

The node ID parameter is not used in this process because the displacements are imported by its coordinate and the new mesh is more refined, so the corresponding nodes have a different number.

The bosses' arrangement is a proposal and changes during this assessment, so their location is uncertain. Given this, the external temperature file imported in the plasma formation load case does not include values to attribute to the bosses and as a lapse in the importation some parts of the geometry of the VV may have the same problem. A temperature linearization is then required to attribute a T different from the default 20ºC to these points and this process is described in the following steps:

1) Use a static structural analysis created before to provide a valid model to the thermal analysis;

2) Create a steady-state thermal analysis using the model referred in last step (the geometry, material properties and mesh used are the same). The external file with the temperature values is used as input and the output consists only in the linearized temperature in all the geometry;

3) Create a static structural analysis using the model referred in step one. The input of the analysis are the temperature values obtained in last step and the external file containing the plasma formation displacements.

The linearized temperature values are imported to the static structural model by node and to each geometry part separately. When the geometry changes, the temperature linearization process needs to be done again. Otherwise the importation is being performed between bodies that don't match or to bodies that no longer exist.

4.4.2.1. Mesh information

The base mesh created for this initial task is the one with less elements used in all this study because it was not converged in any part of the geometry but it is still a relatively fine mesh, so the results evaluated are valid for comparison. It is also visible in table 4.2 that most of the elements created are hexahedral, just as demanded to the software.

Table 0.2 - Mesh node and element number

Nodes	Nodes in the boundaries	Elements	Hexahedral elements	Tetrahedral elements
1339110	40415	357891	321797	36094

The requirement of having a mesh with more nodes that the number of temperature values imported in the plasma formation (1331990) is fulfilled. The same is verified in the boundary surfaces (38644 input displacement values).

4.4.3. Geometry 1

In this sub-chapter the worst load case scenario will be used as setup for all the analyses. A fatigue assessment will be performed in the weld toe and the weld root in the three bosses, using different approximation methods.

The Plasma formation is used as input because it is the most demanding load to the structure, as can be confirmed in chapter 5 of the thesis. The plasma formation analysis created before will be used as a starting point because it already has the linearized temperatures imported to the model and the base mesh that only has to be converged in the interest area. Both weld root and weld toe are areas with geometrical discontinuity due to the 90-degree shape visible at figure 4.3, so the stresses directly evaluated there are not real and have to be obtained with an appropriate approximation method.

The first analysis intends to calculate the type “B” hot-spot stress described in chapter 2, on the weld toe using a quadratic extrapolation of 3 stress values measured at the surface of the VV at a distance of 4, 8 and 12 mm from the weld toe. To apply this method, it is required that the model has a mesh with the element length in this part of the geometry equal or smaller than 4 mm (it’s intended to a model with a fine mesh).

$$\sigma_{hs} = 3\,\sigma_{4\,mm} - 3\,\sigma_{8\,mm} + \sigma_{12\,mm} \tag{4.1}$$

The critical point of the weld toe can be in any of the 3 bosses and anywhere around the boss. Three circles with the radius of 4, 8 and 12 mm counting from the weld toe were drawn around each boss, as can be seen in figure 4.14. This step was done in Ansys SpaceClaim and consisted in creating the 9 circles in the plan of the boss’ top and projecting them onto the VV surface. The projecting tool had to be used because the VV surface is not flat and cannot be used as a sketch plan.

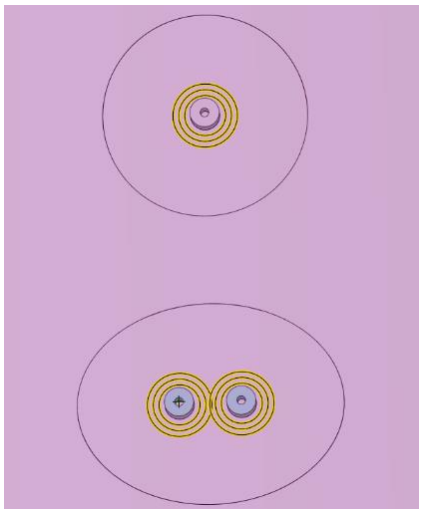

Figure 0.14 - Extrapolation points location in type "B" extrapolation

All the bodies kept the element size defined before except the 2 bodies shown in figure 4.2 (a) where a mesh convergence was performed, using the maximum of the equivalent stress as output value. The initial element size was set as 4 mm because it's the maximum allowed in this approximation method and then decreased until the results convergence is obtained.

With a converged mesh in this area it was possible to evaluate with precision the maximum and minimum principal stresses in the 9 circles drawn before. With the intent to be as conservative as possible, the path with higher ranges between the maximum and minimum principal stresses that result in a higher hot-spot stress was chosen. Back to SpaceClaim software, a line is drawn in the path location to obtain the exact stress value in the 3 intersection of the circles with this line. The highest hot-spot stress value is obtained introducing the 3 principal stress values obtained in equation (4.1) and then corrected for the base material thickness, model temperature and plasticity effects.

In the second analysis performed with the initial geometry is calculated the hot-spot stress in the weld root. The method used was a linearization of all the stresses measured in a path through the base material thickness. This path is a straight line that finishes or starts in the weld root and the pretended stress value in the boss far end will be given automatically by the software, that creates a trend line of the variation along the thickness.

A mesh convergence was performed in the lateral surfaces of the cylinders shown in figure 4.2 (c) because is where the stresses are measured and linearized. Since the edge in the geometry that corresponds to the weld root is a geometrical discontinuity, the equivalent stress values directly evaluated there are not valid and cannot be included in the area to perform the mesh convergence. The von-Mises stress was evaluated in these 3 surfaces to check until what fraction of the thickness it shows a uniform variation, determining the convergence area. Figure 4.15 shows that the stress value increases uniformly until 87% of the thickness, where the maximum value is registered.

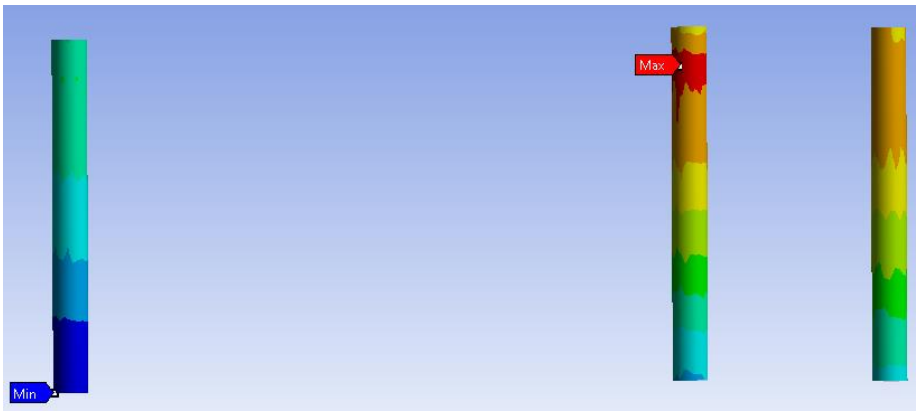

Figure 0.15 - Stress distribution along the thickness

In figure 4.16 is shown the area considered in the convergence that was limited at approximately 80% of the thickness, for conservative reasons. The area delimitation consists I drawing a circle on the outer surface using the projection tool of Ansys SpaceClaim mentioned before. The maximum of the equivalent stress measured in these 3 areas was used as output in the mesh convergence and the parameters varying were the number of divisions in the cylinders' perimeter and the VV thickness.

Figure 0.16 - Area to perform mesh convergence

The critical point of the weld root can be located in any of the 3 bosses and anywhere around the boss. The paths were created all around the 3 bosses in the straight lines that form the mesh. The cylinders perimeter is divided in 22 equal parts in the mesh creation, so 66 paths were created in total.

The value that is going to be linearized is the sum of the bending and the membrane stress evaluated on all points of the paths. The mesh converged when the VV thickness direction was divided in 20 equal parts, so there are 21 nodes in the path to create the trend line. The last point of the path corresponds to the weld root location and always shows the highest stress. The critical

path gives the hot-spot stress value that is then corrected for the base material thickness, model temperature and plasticity effects.

It is not possible to calculate the hot-spot stress in the weld toe using a type “A” extrapolation with this geometry. There are methods available that consist in linear or quadratic extrapolations but all of them need to consider points at a distance of at least the base material thickness dimension that is 60 mm. Using the current boss disposition there is not enough space between the bosses to draw the necessary circles where the principal stresses are evaluated, as shown in figure 4.11. The distance between the 2 bottom bosses is originally 42.5 mm.

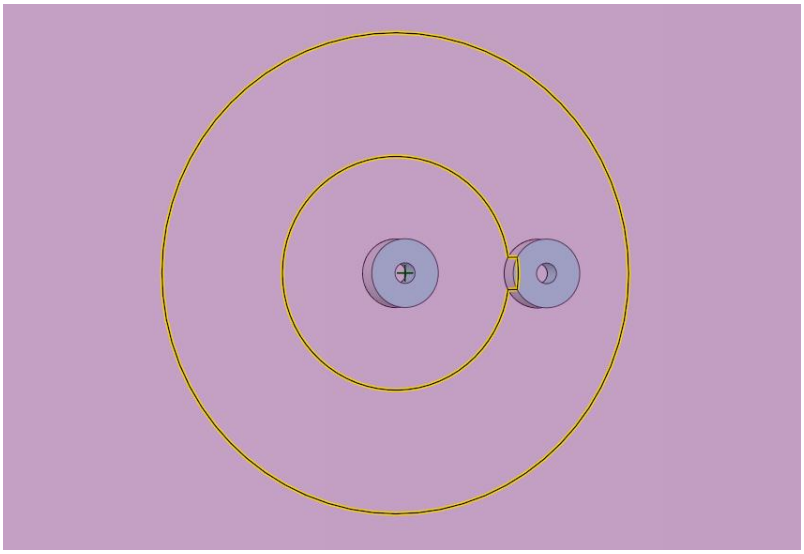

Figure 0.17 - Minimum space required to apply a type “A” extrapolation

4.4.3.1. Mesh information

The 2 new meshes created have more elements than the original one due to the refinement made in the interest areas. The mesh created for the weld toe study has a lot more elements than the second one because the refinement occurred in 2 bodies with bigger volume than the 3 cylinders studied for the weld root. It is also visible in table 4.3 that most of the elements created are hexahedral, just as demanded to the software.

Table 0.3 - Mesh node and element number

	Nodes	Nodes in the boundaries	Elements	Hexahedral elements	Tetrahedral elements
Weld Toe	2403945	40415	639480	581700	57780
Weld root	1437811	40415	368305	336552	31753

The requirement of having a mesh with more nodes that the number of temperature values imported in the plasma formation (1331990) is fulfilled in both cases. The same is verified in the boundary surfaces (38644 input displacement values).

4.4.4. Geometry 2

The plasma formation analysis created in chapter (4.4.2) was also used here as a starting point because it already has the base mesh that only needs to be converged in the interest areas and the material properties.

After applying the geometrical changes described in chapter (4.3.2) a new temperature linearization was required for the external data. The new geometry created has target body parts that don't match with the source data descendant from the first thermal analysis performed.

After this, the procedures to obtain the hot-spot stresses were exactly those described for the previous geometry. This permits a fair results comparison between the 2 geometries. A type "A" extrapolation to calculate the hot-spot stress in the weld toe is applicable here for the same geometrical reason as with the first geometry.

4.4.4.1. Mesh information

The 2 new meshes created have more elements than the original one due to the refinement made in the interest areas. The mesh created for the weld toe study has more element than the second one because the refinement occurred in 2 bodies with bigger volume than the 3 cylinders studied for the weld root. The weld toe analysis has a much lighter mesh than with the previous geometry because the results converged with a higher element size and this is preferable because the analysis gives valid results consuming less time to run. It is also visible in table 4.4 that most of the elements created are hexahedral, just as demanded to the software.

Table 0.4 - Mesh node and element number

	Nodes	Nodes in the boundaries	Elements	Hexahedral elements	Tetrahedral elements
Weld Toe	1757066	40415	458531	417399	41132
Weld root	1415897	40415	363216	331637	31579

The requirement of having a mesh with more nodes that the number of temperature values imported in the plasma formation (1331990) is fulfilled in both cases. The same is verified in the boundary surfaces (38644 input displacement values).

4.4.5. Geometry 3

All the analysis developed in this phase of the fatigue assessment also used the plasma formation analysis created in chapter (4.4.2) as starting point and the temperature linearization had to be repeated for the same reasons as with geometry 2. The procedures adopted were also the same as with the previous geometries but the arrangement of the bosses now allows us to apply a type "A" extrapolation method to calculate the hot-spot stress in the weld toe.

The third analysis performed with this geometry uses a linear extrapolation of 2 stress values measured at the surface of the VV at a distance of 40% and 100% of the base material thickness (24 and 60 mm, respectively) from the weld toe. To apply this method, it is required that the model has a mesh with the element length in this part of the geometry equal or smaller than 40% of the base material thickness (this condition is respected by a large margin in our mesh).

$$\sigma_{hs} = 1.67\ \sigma_{0.4\ t} - 0.67\ \sigma_{1.0\ t} \tag{4.2}$$

The critical point of the weld toe can be in any of the 3 bosses and anywhere around the boss. 2 circles with the radius of 24 and 60 mm counting from the weld toe where drawn around each boss, as can be seen in figure 4.18.

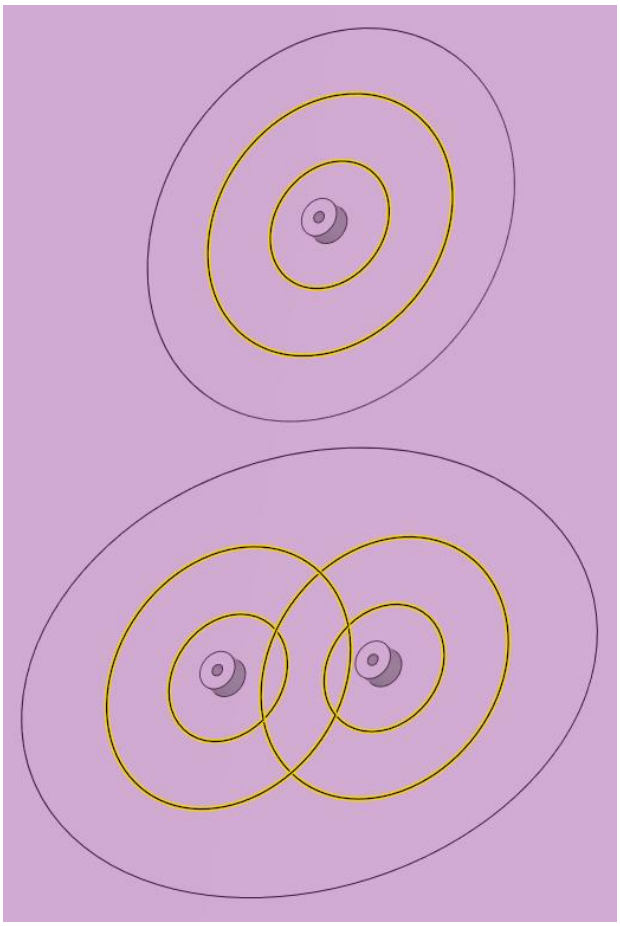

Figure 0.18 - Extrapolation points location in method A

All the bodies kept its element size defined before, except the 2 bodies created in this geometry just like the ones shown in figure 4.2 (a) where a mesh convergence was performed, using the maximum of the equivalent stress as output value. The initial element size was set as 7 mm and decreased until the result values converge.

After the final mesh is obtained the maximum and minimum principal stresses were calculated in the 6 circles drawn before. To obtain the highest value of the hot-spot stress in the weld toe, the path with higher ranges between the maximum and minimum principal stresses was chosen. Back to SpaceClaim software, a line is drawn in the path location to obtain the exact stress value in the 2 intersection of the circles with this line. The highest hot-spot stress value is obtained introducing the 3 principal stress values obtained in equation (4.2) and then corrected for the base material thickness, model temperature and plasticity effects.

4.4.5.1. Mesh information

The refinements performed in the interest areas resulted in the 3 new meshes having more elements than the generic one used as start point. The mesh created for the weld toe study using method “B” has more elements than the other 2 because the refinement occurred in 2 bodies with bigger volume. The mesh created for the weld toe study using method A has a lot less elements than the mesh obtained in method B because despite the refinement has been done in the same 2 bodies, the results converged with a much bigger element size. It is also visible in table 4.5 that most of the elements created are hexahedral, just as asked to the software.

Table 0.5 - Mesh node and element number

	Nodes	Nodes in the boundaries	Elements	Hexahedral elements	Tetrahedral elements
Weld Toe (type “B”)	1958210	40415	514144	467800	46344
Weld root	1435286	40415	367714	336197	31517
Weld Toe (type “A”)	1474289	40415	378026	344532	33494

The requirement of having a mesh with more nodes that the number of temperature values imported in the plasma formation (1331990) is fulfilled in the 3 cases. The same is verified in the boundary surfaces (38644 input displacement values).

4.4.6. Total Usage Factor

After the project requirements are met for the plasma formation load case, it is still necessary to check the feasibility of the third geometry proposed considering all the load cases that the structure will be subject to.

With the third configuration proposed for the bosses, the project safety factor imposed was verified in all the critical weld points, but the safety margin was smaller when using the type “B” extrapolation to assess the fatigue at the weld toe in contact with the boss outer surface. That will be point where this chapter of the fatigue assessment will focus.

The plasma formation stress values were already obtained in the sub-chapter (4.4.5). The load cases used as setup in this chapter are the baking pressure, the plasma disruption combined with a seismic event and the plasma disruption itself. These 3 new analyses use the model created in the last chapter because it already has a converged mesh in the interest area and the procedures are the same described for the first geometry.

4.4.6.1. Mesh information

The mesh used for the software calculation is the same described in last sub-chapter for the type “B” extrapolation method, since only the load setup has changed. Its summary is repeated below.

Table 0.6 - Mesh node and element number

Nodes	Nodes in the boundaries	Elements	Hexahedral elements	Tetrahedral elements
1958210	40415	514144	467800	46344

5 Presentation and analysis of results

The first result to be analysed is the effect of linearizing the temperature distribution provided in an external file for the plasma formation load case. The importance of this step is applied to all the analysis performed in this study and influences all the results. Figure 5.1 shows the difference in the temperature input with and without performing a linear analysis previously to uniform the temperature. In the image of figure 5.1 (b) this step was not done and the bosses have the project reference temperature of 20 ºC.

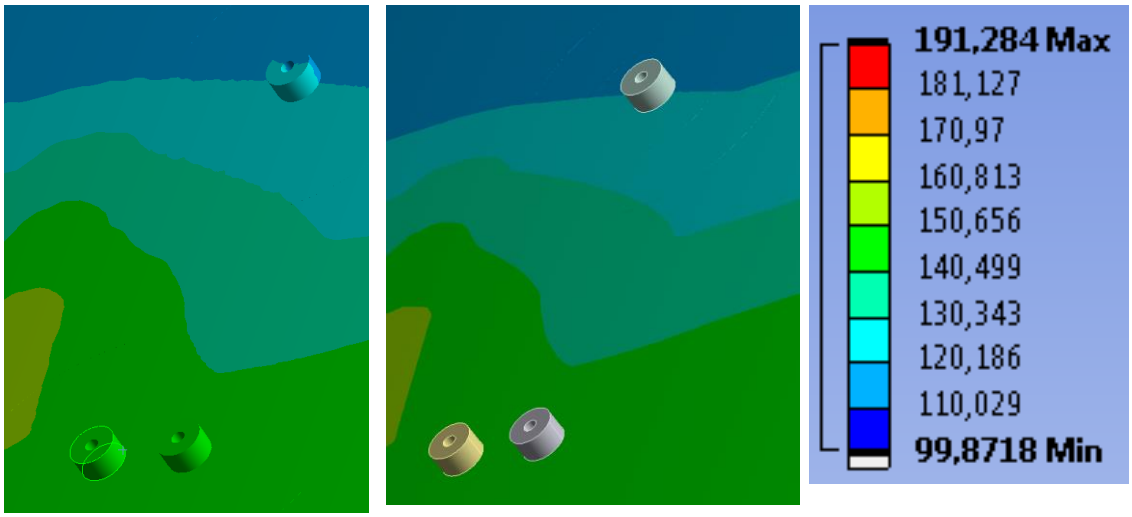

(a) *(b)* *(c)*

Figure 5.1 - Temperature distribution (a) with values attributed to the bosses, (b) with the model reference temperature on the bosses, (c) temperature values [ºC]

This also happens in small areas of the whole geometry that may not get the correct plasma formation temperature but is only visually identified in the bosses. Figure 5.2 shows the result in the equivalent stress evaluated in the bosses. It is visible that the distribution has changed, but also the maximum value in the edge of the interface with the VV. Instead of a maximum equivalent stress value of 242.4 MPa, a peak stress of 522.5 MPa is obtained if the uniformization is not carried out.

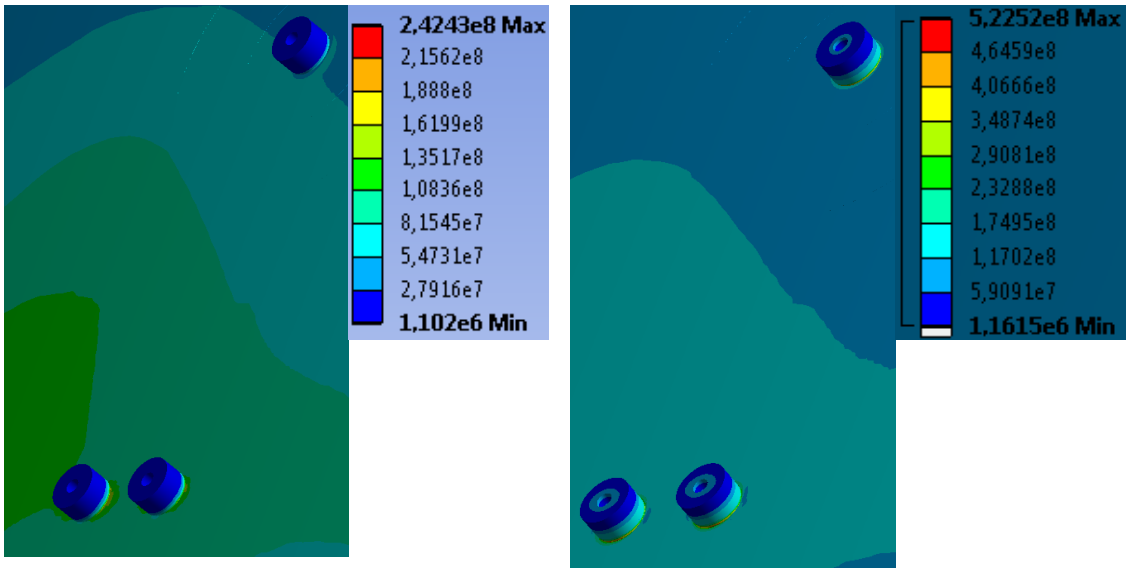

(a) *(b)* *(c)* *(d)*

Figure 5.2 - (a) Equivalent stress in the bosses with a temperature linearization, (b) corresponding stress values [Pa], (c) Equivalent stress in the bosses without a temperature linearization, (d) corresponding stress values [Pa]

5.1. Determining the worst load case scenario

In this section the stress distributions of all load cases applicable to the geometry will be compared, using the initial geometry provided. The output used in the comparison is the equivalent von-Mises stress. All the geometry points are assessed in this step to make sure that the most harmful load for the structure is chosen. The equivalent stress distribution for each load case scenario is illustrated in figures 5.3 to 5.9.

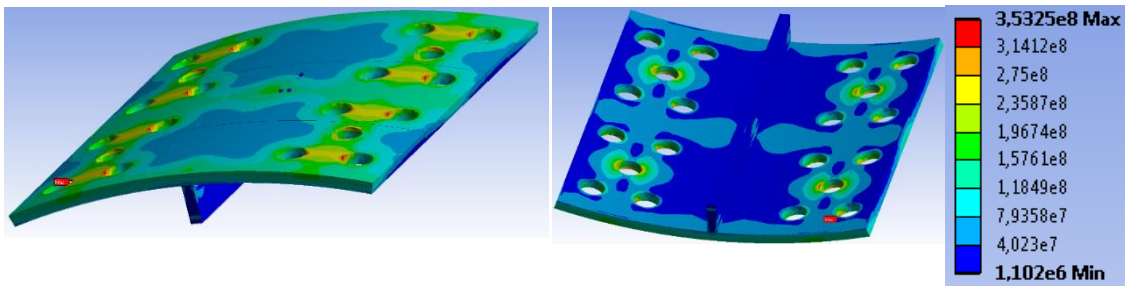

(a) *(b)* *(c)*

Figure 5.3 - Stress distribution with the load plasma formation (a) inside the VV, (b) outside the VV, (c) values [Pa]

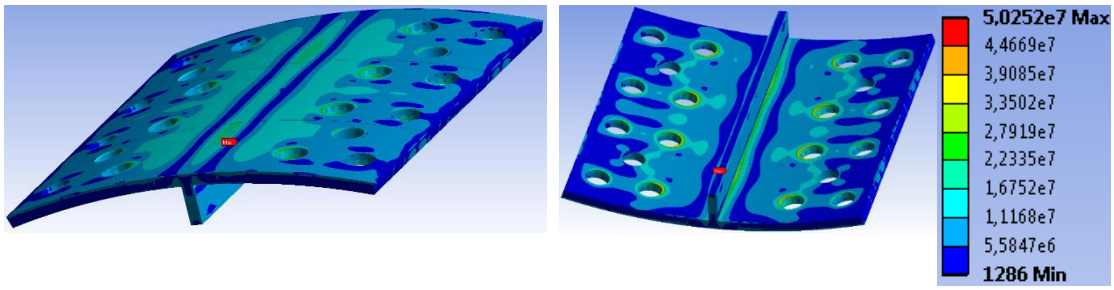

(a) (b) (c)

Figure 5.4 - Stress distribution with the load normal operation pressure (a) inside the VV, (b) outside the VV, (c) values [Pa]

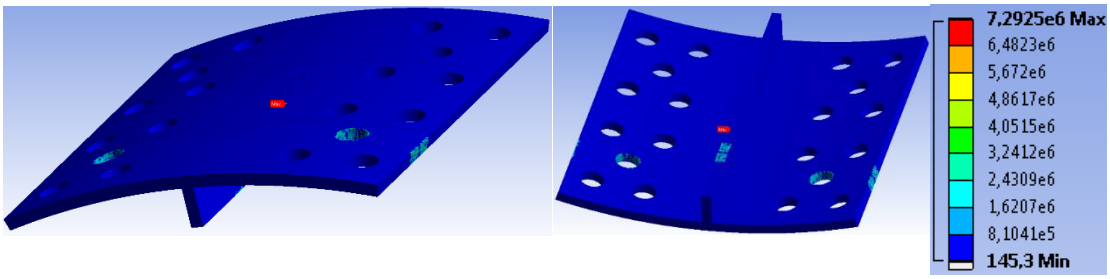

(a) (b) (c)

Figure 5.5 - Stress distribution with the load normal operation temperature (a) inside the VV, (b) outside the VV, (c) values [Pa]

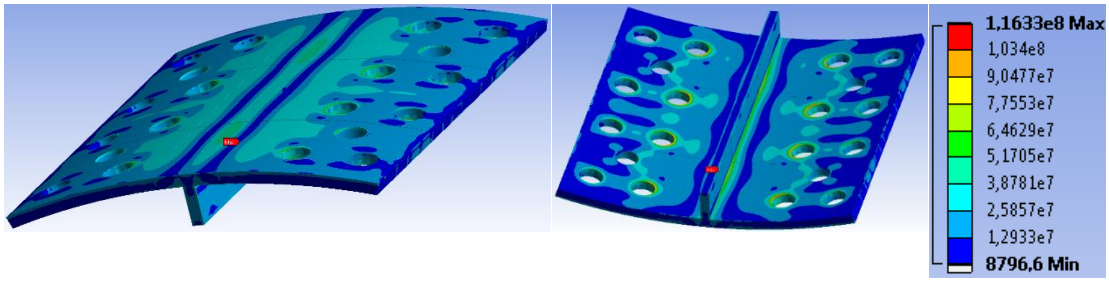

(a) (b) (c)

Figure 5.6 - Stress distribution with the load baking pressure (a) inside the VV, (b) outside the VV, (c) values [Pa]

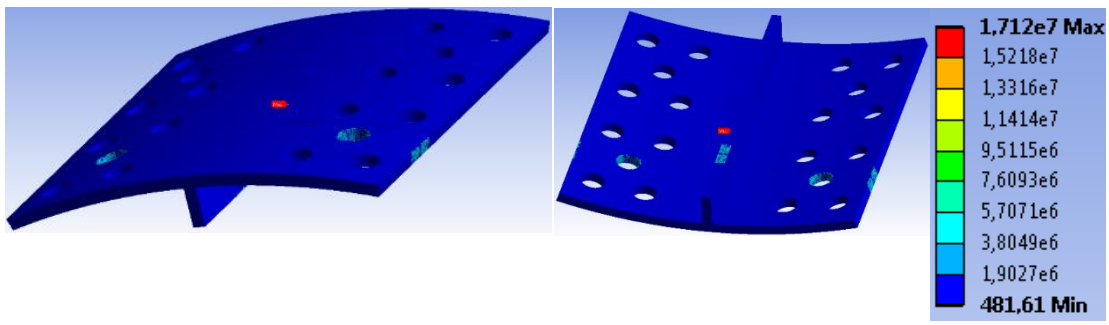

(a) (b) (c)

Figure 5.7 - Stress distribution with the load baking temperature (a) inside the VV, (b) outside the VV, (c) values [Pa]

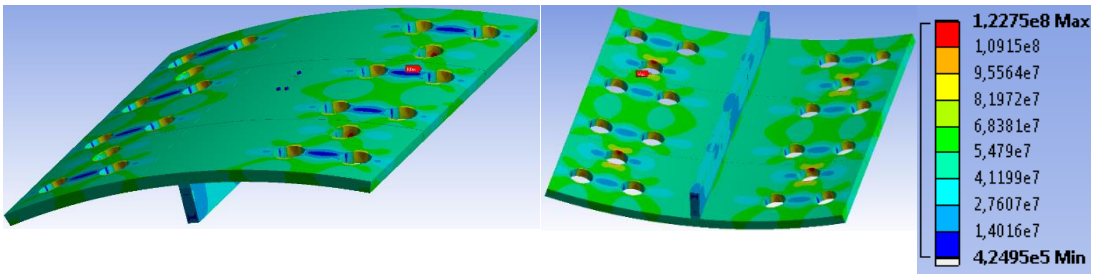

(a) *(b)* *(c)*

Figure 5.8 - Stress distribution with the load plasma disruption (a) inside the VV, (b) outside the VV, (c) values [Pa]

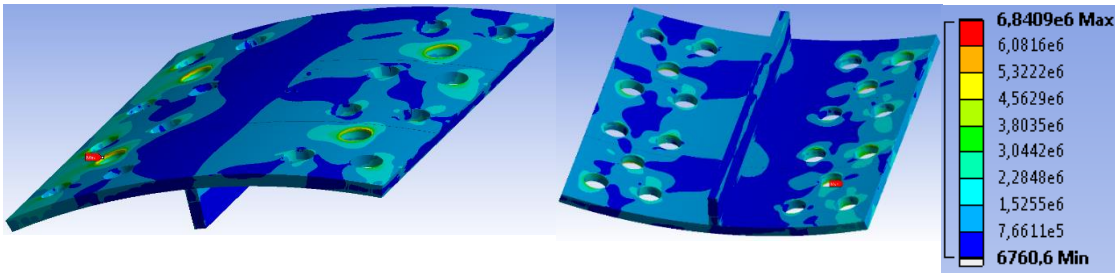

(a) *(b)* *(c)*

Figure 5.9 - Stress distribution with the load seismic event (a) inside the VV, (b) outside the VV, (c) values [Pa]

Scoping the results just in the area around the bosses and the bosses itself, the stress distribution follows the pattern of figure 5.10 for all the load cases.

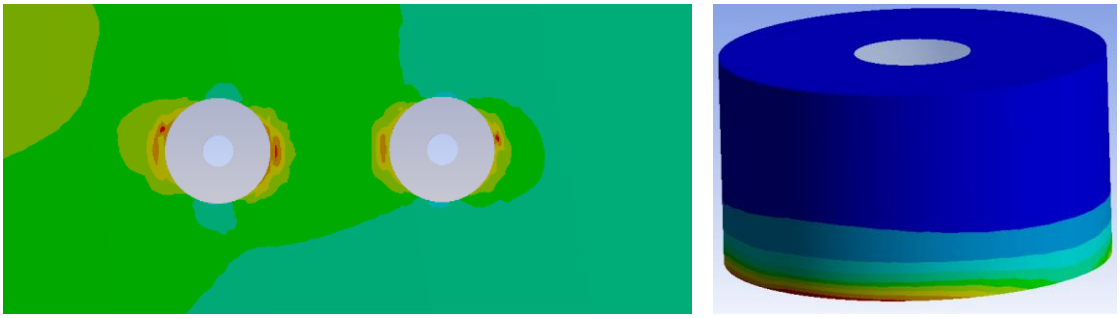

(a) *(b)*

Figure 5.10 - Stress distribution (a) around the bosses, (b) in the bosses

The maximum value of stress verified in the 3 geometry areas for all the 7 load cases is resumed in table 5.1

Table 5.1 - Stress distribution in the geometry

Load Case	Maximum stress in whole geometry [MPa]	Maximum stress around the bosses [MPa]	Maximum stress in the bosses [MPa]
Plasma formation	353.3	249.7	242.4
Normal operation pressure	50.3	17.4	11.9
Normal operation temperature	7.3	0.1	0.2
Baking pressure	116.3	40.2	27.4
Baking temperature	17.1	0.1	0.4
Plasma disruption	122.8	85.2	84.1
Seismic event	6.8	1.4	1.6

Comparing the results, the plasma formation is by far the most demanding load to the structure in all the areas evaluated. It has to be taken in account that none of the values of table 5.1 is real (or precise) because they are obtained in local geometrical discontinuities. The highest value evaluated in the whole geometry always corresponds to a 90-degree shape (exactly or approximately) like, for example, the edge of the wholes of the VV far from the bosses. Those are boundary surfaces where the displacements are applied and are part of the sub-modelling technique surface, so they do not correspond to the real shape of the VV wall. The highest value evaluated around the bosses and in the bosses correspond to hot-spot. Its value is not accurate and is corrected in this study with the surface extrapolations.

Therefore, the peak stress values obtained do not allow a quantitative comparison, but qualitatively they prove that the plasma formation is the most harmful load for the structure.

Some of the stress values obtained are above the yield stress for the material but nothing can be concluded regarding plastic deformations, because of the same reasons stated before.

5.2. Geometry 1

5.2.1. Type “B” weld toe

The first step in this phase of the assessment is to perform a mesh convergence in the areas that will be studied.

The type “B” extrapolation method is used to calculate the hot-spot stress in the weld toe in contact with the boss. It uses stress values at the VV inner surface and the convergence was performed only in the body part that contains that surface. The initial element size was set as 4 mm (it is the maximum length allowed in this extrapolation method) and decreases until the equivalent stress

values converge. The convergence was performed in the 9 circles of figure 4.8 and the result is visible in figure 5.11.

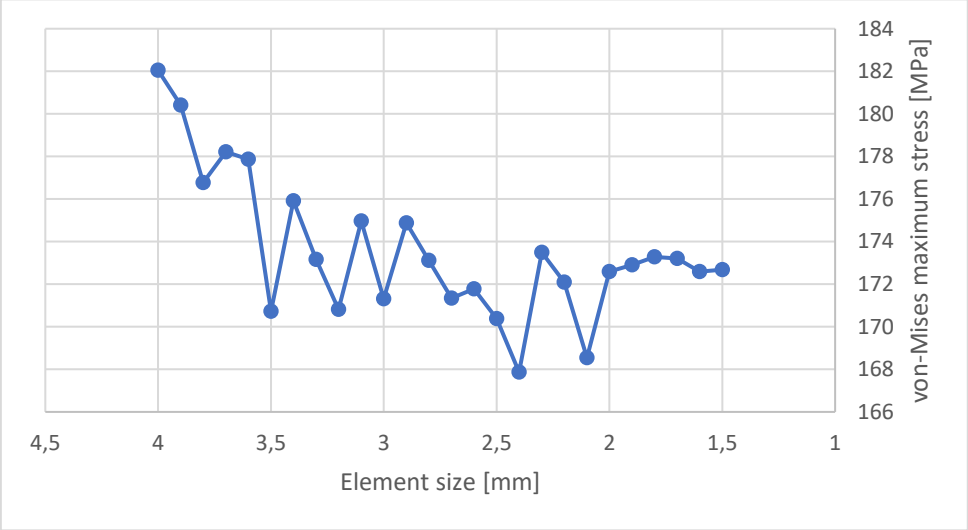

Figure 5.11 - Mesh convergence for type "B" extrapolation

The results started to converge with an element size of 2 mm, so this was the size used in the extrapolation. Evaluating the maximum and minimum principal stress in the circles of figure 4.8, the critical path obtained has the principal stress values displayed by node in table 5.2.

Table 5.2 - Maximum and minimum principal stress

	Max principal stress [MPa]	*Min principal stress [MPa]*	*Stress range [MPa]*
Node 1 (4 mm)	-0.06	-195.4	195.4
Node 2 (8 mm)	0.06	-184	184.1
Node 3 (12 mm)	0.02	-182.1	182.2

The stress range is the difference in modulus between the maximum and minimum stress in each node. The stress range values are introduced in equation (2.18) and the hot-spot stress is obtained as 216.06 MPa.

The fatigue assessment in this study follows the standard EN 13445-3 [3]. This standard is based in experimental results that were performed in specimens with a thickness of 25 mm at 100 ºC. To apply the standard in other studies, correction factors need to be applied to the hot-spot stress obtained if the material's temperature and thickness are above these values.

Equation (5.1) shows the expression to obtain the mean temperature of the structure in case it is higher than 100 ºC and equation (5.2) is used to calculate the correction factor to apply to the hot-spot stress.

$$T^* = 0.75\,T_{max} + 0.25\,T_{min} \tag{5.1}$$

$$f_{T^*} = 1.043 - 0.00043\,T^* \tag{5.2}$$

T* is the mean temperature value and T_{max} and T_{min} are the maximum and minimum temperature value measured in the structure, respectively.

The thickness correction factor is calculated with equation (5.3).

$$f_{ew} = \left(\frac{25}{e_n}\right)^{0.25} \tag{5.3}$$

e_n is the thickness of the base material plate studied.

With a maximum and minimum temperature of 191 and 190 ºC, respectively, in the plasma load, a correction factor of 0.9707 is obtained. The correction factor 0.803 was calculated for a thickness of 60 mm in the VV walls. The corrected stress range of the hot-spot is obtained from equation (5.4).

$$\Delta\sigma_{corr} = \frac{\Delta\sigma_{hs}}{fT^*.f_{ew}} \tag{5.4}$$

After applying the correction factor, the stress range value is 277.1 MPa.

The S-N curve followed in the standard plots the stress range in the weld details with the number of cycles to failure as shows figure 5.12. The graphic has a curve for each FAT-class. The FAT-32 in the bottom is the most conservative class and the FAT-100 is the class that allows the highest stress range for the value of N.

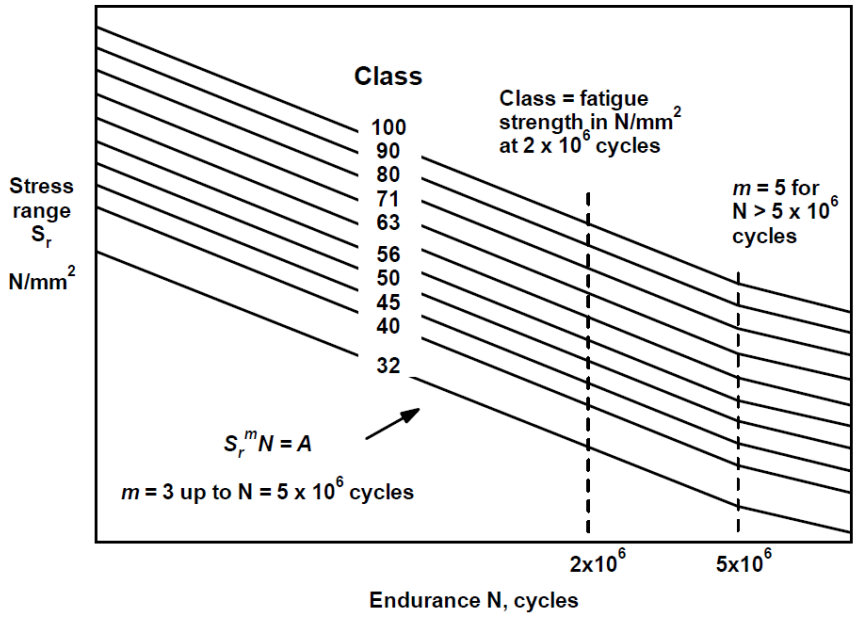

Figure 5.12 - S-N curve for weld details [3]

The maximum number of cycles for the stress range calculated can be determined analytically using equation:

$$N = \frac{C}{\Delta\sigma_{corr}^{3}} \tag{5.5}$$

where C is a constant that gives the information about the FAT-class used and is obtained from table 5.3.

Table 5.3 - Design parameters for each FAT-class [27]

Class	Constants of $\Delta\sigma_R$ - N curve*				Stress range at N cycles, MPa	
	For $10^2 < N < 5x10^6$		For $5x10^6 < N < 10^8$		$N = 5 \times 10^6$	$N = 10^8$
	m_1	C_1	m_2	C_2	$\Delta\sigma_D$	$\Delta\sigma_{Cut}$
100	3,0	$2,00 \times 10^{12}$	5,0	$1,09 \times 10^{16}$	74	40
90	3,0	$1,46 \times 10^{12}$	5,0	$6,41 \times 10^{15}$	66	36
80	3,0	$1,02 \times 10^{12}$	5,0	$3,56 \times 10^{15}$	59	32
71	3,0	$7,16 \times 10^{11}$	5,0	$1,96 \times 10^{15}$	52	29
63	3,0	$5,00 \times 10^{11}$	5,0	$1,08 \times 10^{15}$	46	26
56	3,0	$3,51 \times 10^{11}$	5,0	$5,98 \times 10^{14}$	41	23
50	3,0	$2,50 \times 10^{11}$	5,0	$3,39 \times 10^{14}$	37	20
45	3,0	$1,82 \times 10^{11}$	5,0	$2,00 \times 10^{14}$	33	18
40	3,0	$1,28 \times 10^{11}$	5,0	$1,11 \times 10^{14}$	29,5	16
32	3,0	$6,55 \times 10^{10}$	5,0	$3,64 \times 10^{13}$	24	13
* For $E = 2,09 \times 10^5$ MPa						

The hot-spot stress in the weld toe is assessed using the class FAT-71 and the design point is in the first part of the curve (before N = $5x10^6$ cycles) where the slope is m = 3, so the constant is C = $7.16x10^{11}$. Solving equation (5.5) the maximum allowed value of N is 33651 cycles and corresponds to a safety factor of 1.

The safety margin in this study is determined with a parameter called usage factor (UF) that is the inverse of the normal safety factor used in engineering (n). This means that the design is more conservative if lower usage factor values are obtained. For each load case of this assessment, it is required that the usage factor is below 0.05 and it is obtained with the equation:

$$UF = \frac{N_E}{N_{max}} \tag{5.6}$$

where N_E is the number of events required during all the fatigue time of the structure and N_{max} is the maximum number of cycles allowed for the stress range evaluated.

For this load case, the number of events that the structure need to support is 2591. Solving the equation (5.6) a value of 0.077 is obtained for the usage factor, which means the project requirements are not met in the weld toe for the initial geometry.

5.2.2. Weld root

The hot-spot in the weld root was calculated using the extrapolation method through the thickness and the convergence was performed only in the outer surface of the 3 body parts described in figure 4.2(c). The element size was defined during the mesh creation by setting a number of divisions along the VV thickness and a number of divisions around the cylinder perimeter. These 2 numbers were the parameters to vary in the mesh convergence and the strategy used was to vary the number of divisions on the cylinder perimeter for each number of divisions of the thickness. Basically, several mesh convergences were performed (1 for each element length through the thickness). Figure 5.13 shows the convergence that produced better results. The element size around the perimeter is varying with the thickness divided in 20 equal parts (3 mm).

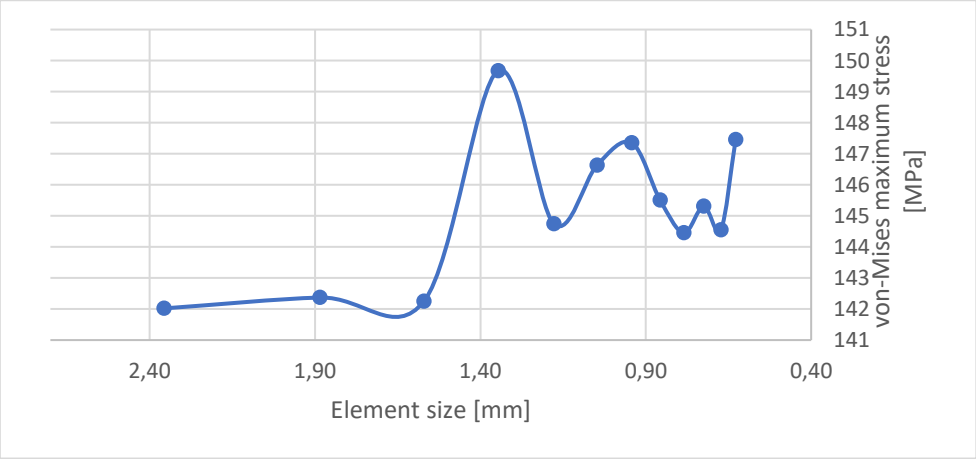

Figure 5.13 - Mesh convergence for extrapolation through the thickness

The results have a small variation for the element sizes studied, but they reach a more stable converge with an element size of 0.9 mm (22 divisions around the perimeter), so this was the element size used in the extrapolation. The software evaluated the linearized sum of the membrane and bending stress in all the path around the cylinder, like the one illustrated in figure 5.14.

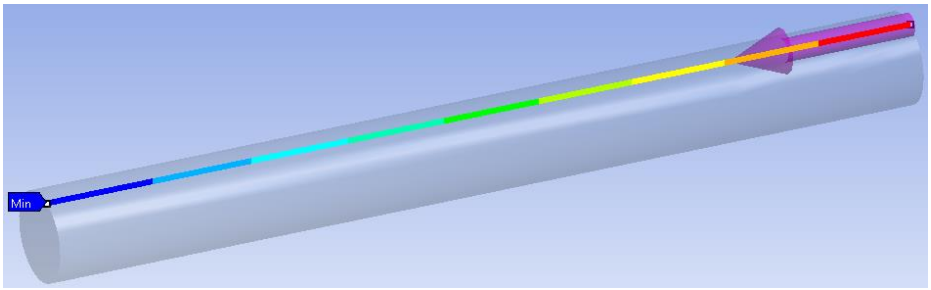

Figure 5.14 - Path along the VV thickness

The maximum value obtained for the end of the path that corresponds to the weld root hot-spot stress was 161.98 MPa. The correction factor are applied to the hot-spot stress just like was done in the weld toe and a stress range of 207.7 MPa is obtained.

The hot-spot stress in the weld root is assessed using the class FAT-63 so the constant to use in equation (5.5) is $C = 5.0 \times 10^{11}$. The maximum allowed value of N is 55803 cycles.

Applying equation (5.6) the usage factor in the weld root is 0.0464, which is below the limit of 0.05 and meets the project requirements imposed with the initial geometry.

5.3. Geometry 2

With the second geometry the extrapolation methods and procedures were exactly the same as with the initial geometry, for each weld location. This is essential to make a proper comparison because there should be no more variables to consider, except the increased distance between the bosses. Only the final results obtained in each step are exhibited in this sub-chapter.

5.3.1. Type “B” weld toe

The convergence of results to calculate the stress range in the weld toe is illustrated in figure 5.15.

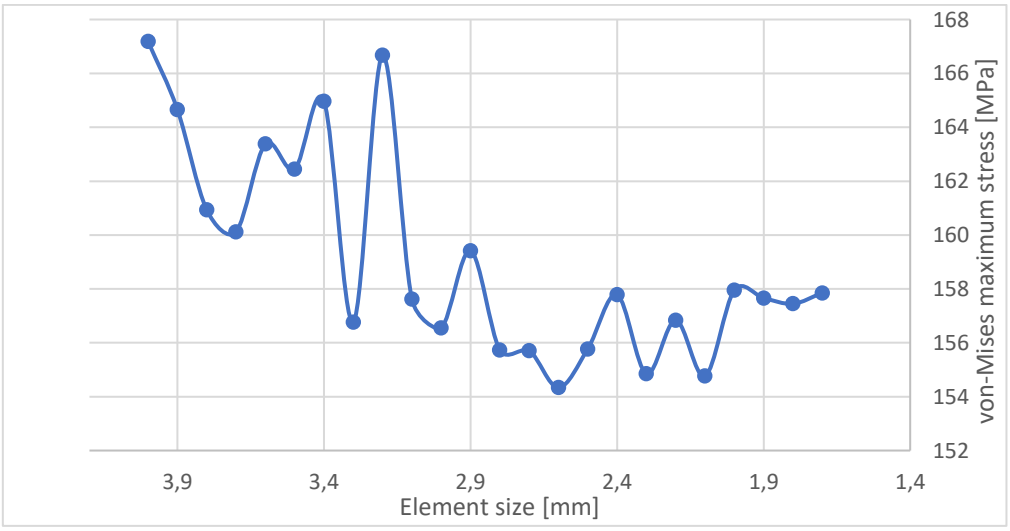

Figure 5.15 - Mesh convergence for type “B” extrapolation

The results started to converge with an element size of 2.7 mm, so this was the size used in the extrapolation. The principal stress values evaluated in the areas of interest are displayed by node in table 5.4.

Table 5.4 - Maximum and minimum principal stress

	Max principal stress [MPa]	*Min principal stress [MPa]*	*Stress range [MPa]*
Node 1 (4 mm)	0.79	-179.35	180.1
Node 2 (8 mm)	0.2	-169.23	169.4
Node 3 (12 mm)	0.01	-167.43	167.4

The hot-spot stress range obtained using equation (2.18) is 199.58 MPa. After applying the correction factor, the stress range value is 255.9 MPa. Solving the equation (5.5) the maximum allowed value of N is 42726 cycles. Solving the equation (5.6) a value of 0.0607 is obtained for the usage factor, which means the project requirements are not met in the weld toe for this geometry either.

5.3.2. Weld root

The mesh convergence process that produced better results is represented in figure 5.16. The element size around the perimeter is varying with the thickness divided in 30 equal parts (2 mm).

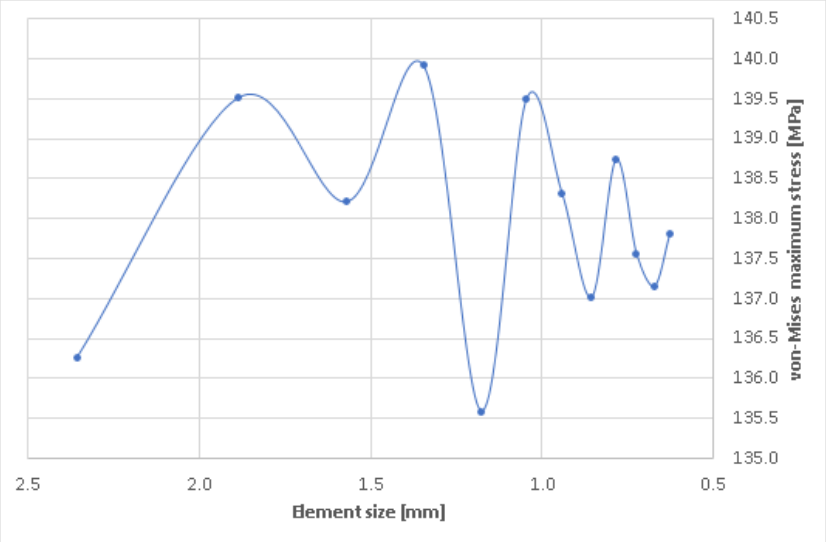

Figure 5.16 - Mesh convergence for extrapolation through the thickness

The results converge for a very small variation with an element length of 0.95 mm (20 divisions around the perimeter), so this was the element size used in the extrapolation. The hot-spot stress obtained was 151.6 MPa. After applying the correction factors, a stress range of 194.4 MPa is obtained in the weld root. Solving the equation (5.5) the maximum allowed value of N is 68154

cycles. Solving the equation (5.6) a value of 0.0381 is obtained for the usage factor. The previous arrangement for the bosses was already compliant with the requirements for the weld root, but the safety margin has increased now.

The decrease in both hot-spot stress ranges confirms that the existing stresses in the base plate, near the weld joints, have a strong influence in the stress distribution of the boss.

5.4. Geometry 3

The extrapolation methods used in the previous geometries are also applied in the third geometry with the same procedures, so only the final results obtained in each step will be exhibited.

The difference with this geometry is that another kind of extrapolation method is now possible to apply, thus enhancing the accuracy of the fatigue assessment. The results of a type "A" extrapolation will also be presented.

5.4.1. Type "B" weld toe

The convergence of results to calculate the stress range in the weld toe is illustrated in figure 5.17.

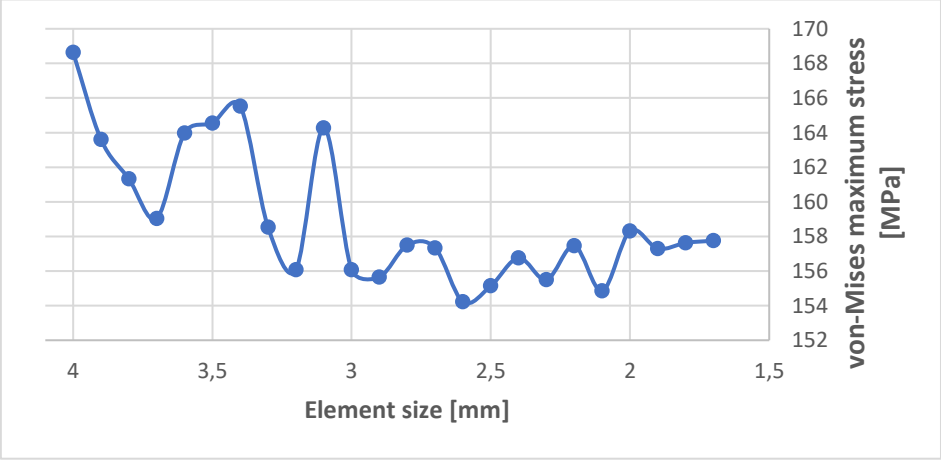

Figure 5.17 - Mesh convergence for type "B" extrapolation

The results started to converge with an element size of 2.5 mm, so this was the length used in the extrapolation. The principal stress values evaluated in the areas of interest are displayed by node in table 5.5.

Table 5.5 - Maximum and minimum principal stress

	Max principal stress [MPa]	*Min principal stress [MPa]*	*Stress range [MPa]*
Node 1 (4 mm)	-1.09	-175.28	174.19
Node 2 (8 mm)	-0.03	-169.19	169.16
Node 3 (12 mm)	0.03	-167.93	167.96

The hot-spot stress range obtained using equation (2.18) is 183.04 MPa. After applying the correction factor, the stress range value is 234.7 MPa. Solving the equation (5.5) the maximum allowed value of N is 55486 cycles. Solving the equation (5.6) a value of 0.0468 is obtained for the usage factor, which means the project requirements are now met in the weld toe with the third geometry.

5.4.2. Weld root

The mesh convergence process that produced better results is represented in figure 5.18. The element size around the perimeter is varying with the thickness divided in 22 equal parts (2.7 mm).

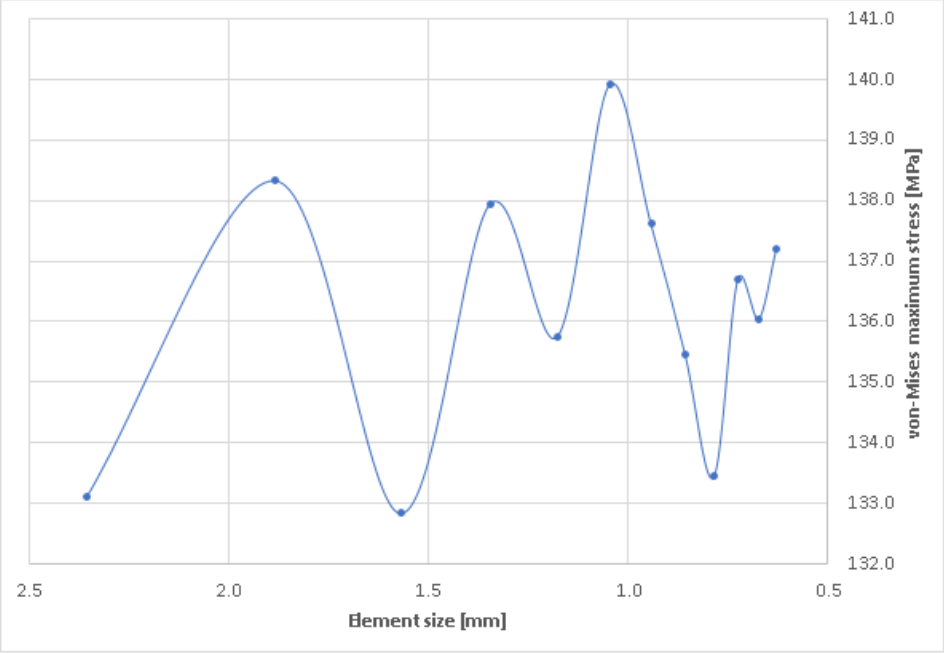

Figure 5.18 - Mesh convergence for extrapolation through the thickness

The results converge for a very small variation with an element length of 0.75 mm (28 divisions around the perimeter), so this was the element size used in the extrapolation.

The hot-spot stress obtained was 148.24 MPa. After applying the correction factors, a stress range of 190.1 MPa is obtained in the weld root. Solving the equation (5.5) the maximum allowed

value of N is 72815 cycles. Solving the equation (5.6) a value of 0.0356 is obtained for the usage factor. With the small decrease in the hot-spot stress, the safety margin as slightly decreased also as expected.

The decrease in both hot-spot stress ranges suggests that the proximity of a boss to a geometrical discontinuity influences a lot the stress distribution and peaks around the boss. Although the peak stress evaluated directly in the weld toe edge is not precise, it exists and affects the surrounding structure.

5.4.3. Type “A” weld toe

The type “A” extrapolation method allows to calculate the hot-spot in the weld toe in contact with VV. It uses stress values at the VV inner surface and the convergence was performed only in the body part that contains that surface. The initial element size was set as 5 mm in the 2 body parts that surround the bosses and then decreases until the equivalent stress values converge. The convergence was performed in the 6 circles of figure 4.12 and the result is visible in figure 5.19.

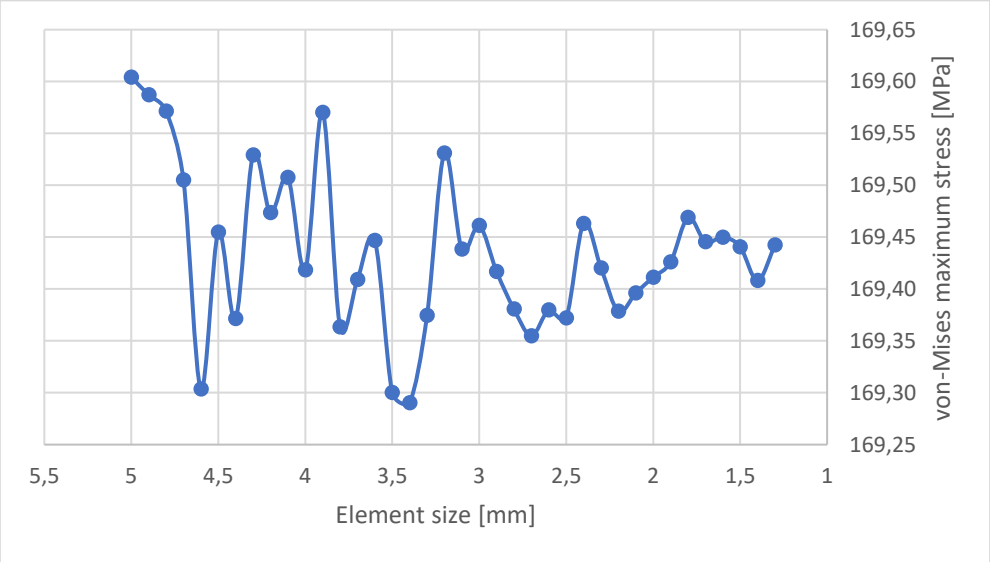

Figure 5.19 - Mesh convergence for type “A” extrapolation

All the points of the graphic are converged because the variation is insignificant, so it means the results start converging for an element length larger than 5 mm. Higher values could have been tested to discover the highest value that gives good results but there is no need because this mesh does not create a too heavy model and the transition in element size from the surrounding to the bosses is smooth. By evaluating the maximum and minimum principal stress in the circles of figure 4.12, the critical path obtained has the principal stress values displayed by node in table 5.6.

Table 5.6 - Maximum and minimum principal stress

	Max principal stress [MPa]	*Min principal stress [MPa]*	*Stress range [MPa]*
Node 1 (24 mm)	-0.05	-172.24	172.19
Node 2 (60 mm)	0	-183.51	183.51

The stress range is the difference in modulus between the maximum and minimum stress in each node. The stress range values are introduced in equation (2.16) and the hot-spot stress is obtained as 164.61 MPa. After applying the correction factors, the stress range value is 211.1 MPa.

The hot-spot stress in the type “A” weld toe is assessed using the class FAT-71 and the design point is in the first part of the curve (before $N = 5x10^6$ cycles) where the slope is m = 3, so the constant is $C = 7.16x10^{11}$. Solving equation (5.5) the maximum allowed value of N is 76118 cycles and corresponds to a safety factor of 1.

Solving the equation (5.6) a value of 0.034 is obtained for the usage factor, which means the project requirements are met in the weld toe in contact with the VV.

This method was not applicable in the other geometries so it is not possible to know if the result would be a usage factor below the limit of 0.05. The fact that it is confirmed by a comfortable margin in the safest geometry assessed in this study is enough to approve this weld zone.

All the usage factors calculated are gathered in table 5.7, so it is easier to compare the 3 geometries and quantify the improvement.

Table 5.7 - Usage factor values

	Type “B”	Through thickness	Type “A”
Geometry 1	0.077	0.0464	
Geometry 2	0.0607	0.0381	
Geometry 3	0.0468	0.0356	0.034

The third geometry studied has a usage factor below the limit of 0.05 in all the weld locations, so the structure can tolerate the plasma formation loads within the safety coefficient required. Since it is the most demanding load by far it means that it can support all the loads, individually. In the next sub-chapter, the usage factor is calculated for all the other loads and all the values are summed to check if the total is below the limit of 0.1. This will be assessed using a type “B”

extrapolation for the weld toe in contact with the boss, since it is the weld detail with smaller safety margin or the most critical weld point.

Figure 5.20 shows a comparison between the variation of the peak stress evaluated directly by Ansys in the weld toe for the 3 geometries studied and the variation of the hot-spot stress extrapolated for the boss weld toe. This extrapolation method was chosen for the comparison because it has the biggest fluctuation among the geometries. The hot-spot is decreases almost by the same value in the geometrical optimizations. The peak stress evaluated numerically has a larger reduction in the first geometry change than in the second. The reason behind this must be the definition of structural stress in chapter (2.3): this kind of evaluation considers all stress raising effects of a structural detail except those due to the local weld profile itself. By ignoring the local notch effect, the structural stress reflects better the other factors and changes.

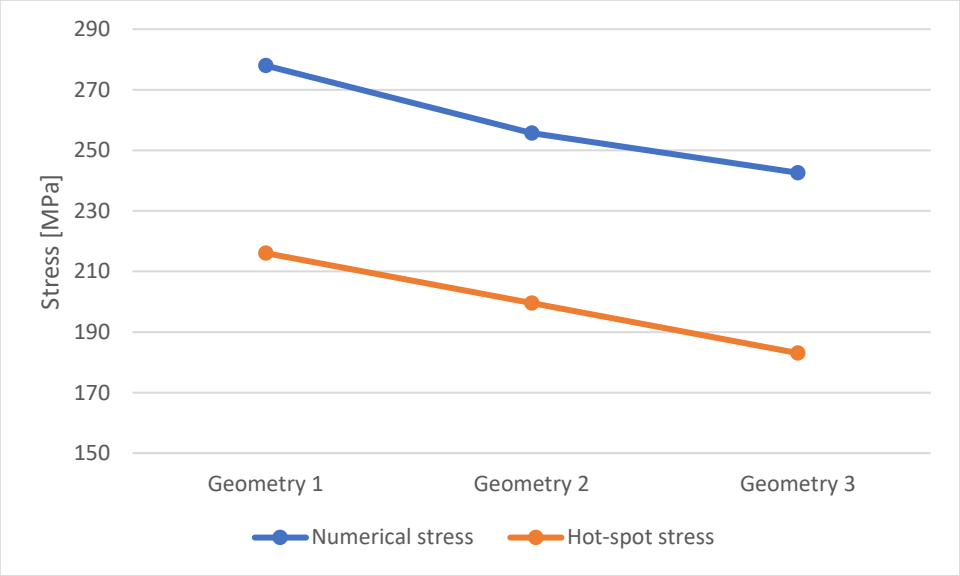

Figure 5.20 - Comparison between hot-spot and local stress

5.5. Total Usage Factor

The different loads that are supported by the VV were categorized and grouped according to its nature. The number of events that will occur during the machine life was also attributed to these groups, as described [28]:

- Nuclear heating: composed by the plasma formation scenario. Consists in 2591 events in total;
- Pressure envelope: consists in the normal operation and the baking pressure load. Consists in 800 events in total and only the baking is considered because it is more demanding to the components;
- Electro-magnetic envelope: all EM transient events have been grouped and are represented by the plasma disruption. It is the transient that generates maximum peak stresses in the VV inner shell. The events number was set as 3850;
- Seismic envelope: includes all the types of seismic loads. Consists in 350 events in total and is composed by the seismic event and the plasma disruption at the same time.

The usage factor for the plasma formation, considering the events number, was calculated before. Its model is used as a base for the other 3 envelopes because only the loads change and the previous mesh convergence is valid.

The principal stress values evaluated around the bosses for each load envelope are displayed by node in table 5.8, 5.9 and 5.10.

Table 5.8 - Maximum and minimum principal stress in baking pressure

	Max principal stress [MPa]	*Min principal stress [MPa]*	*Stress range [MPa]*
Node 1 (4 mm)	35.18	-0.16	35.34
Node 2 (8 mm)	33.55	-0.026	33.58
Node 3 (12 mm)	33.57	-0.004	33.57

Table 5.9 - Maximum and minimum principal stress in plasma disruption

	Max principal stress [MPa]	*Min principal stress [MPa]*	*Stress range [MPa]*
Node 1 (4 mm)	15.03	-49.76	64.79
Node 2 (8 mm)	16.87	-46.15	63.02
Node 3 (12 mm)	17.35	-44.91	62.26

Table 5.10 - Maximum and minimum principal stress in seismic events and plasma disruption together

	Max principal stress [MPa]	*Min principal stress [MPa]*	*Stress range [MPa]*
Node 1 (4 mm)	14.97	-50	64.97
Node 2 (8 mm)	16.88	-46.1	62.98
Node 3 (12 mm)	17.37	-44.92	62.29

The hot-spot stress range is calculated using equation (2.18) and then corrected to consider the model thickness and temperature. The maximum allowed cycles and the usage factor are obtained from equation (5.5) and (5.6). All these values are listed in table 5.11.

Table 5.11 - Calculation of usage factor

Envelope	*Hot-spot stress [MPa]*	*Corrected stress range [MPa]*	N_{max}	*Usage factor*
Baking pressure	38.9	50.6	5526643	0.0001
Plasma disruption	67.6	84.1	1203718	0.0032
Seismic event and plasma disruption	68.3	85	1165886	0.0003

These 3 usage factor values are added up with the plasma formation value to obtain the project total usage factor of 0.0504. This result is around half of the limit imposed so the structural integrity of the welds are ensured for this load and number of cycles proposed.

6 Conclusions

After the work developed in this study and after the result comparison that is described in chapter 5, the main conclusions are listed below:

- The equivalent von-Mises stress only has positive values because the results are represented in modulus, but if the principal stresses are evaluated in any part of the geometry, the peak values are mostly negative. This makes sense because the structure has a high value of temperature in most of the load scenarios and tends to expand, resulting in compressive loads because it is constrained by itself;
- The geometry deformation is not a good tool to measure and quantify the improvements because they are mostly imposed by the displacements input files. The deformation values are not used normally in the mesh convergence because these values are easier to converge than the stress values. In this case it is even less advisable;
- A small load applied on any part of the geometry does not create a noticeable stress peak in the geometrical discontinuity of the weld geometry. The higher the loads on the model, the greater the stress variance between the weld and its surroundings. A plausible conclusion is that the stress values result from the displacements, temperatures, pressure and acceleration applied in the model (and not from the weld notch effect) and are amplified by the geometrical discontinuities, leading to the peak values;
- As expected, the pre-existing stress in the VV wall before the bosses are added to the model, have the greatest contribution to the peak stress in the weld. The stress range decreases when the critical bosses were moved to a less demanded zone of the VV, and this should be the procedure in future improvements of the geometry;
- The proximity between 2 bosses affects the stress range in its welds, as was noticed with geometry 3, since the stress values got lower for the same inputs. The stress peak from the notch effect of the surrounding bosses is one of the major contributions for the hot-spot stress;
- The plasma formation loads proved to be the most harmful load case by a considerable margin, which is supported by the previous conclusion since it is one of the loads with higher temperature values;
- The usage factor obtained with the third geometry and considering only the plasma formation is almost the same of the total usage factor that sums all the load envelopes. This is verified because in addition to the other load scenarios being less demanding, some of them are also applied less times to the structure, resulting in a greater margin to the maximum number of cycles allowed;

- When the fatigue assessment is carried out on the third geometry proposed, the welded joints respect the overall design requirements by a large margin in the weld root and in the weld toe in contact with the VV wall, but only a small margin is verified for the weld toe in contact with the boss lateral surface. It must be taken in consideration that the values imposed have a safety coefficient of n = 20 (the safety coefficient is the inverse of the usage factor) before the mechanical failure occurs, so the result is conservative;
- When the external loads are added to the model it is expected that the stress values in the weld critical points increase, but when the geometry is updated with the correct shape of the weld, the geometrical transition from the VV wall to the boss becomes smoother and the notch effect decreases, leading also to a decrease in the stress values at the critical points. This balance may be negative, meaning that the losses due to the external loads added overcome the gains of the weld shape, but new geometries can be tested then;
- The methodology used is very specific for this case, but it can be applied in other examples, by changing the correction factors, the extrapolation methods or the standard(s) followed.

Future work

The project requirements were met in the end of this work and the objectives were completed but some future tasks are needed for it to better represent reality and contribute to the work in ITER. This is the list of the suggested and advised work:

- Include external loads like screw pre-tension in the bosses, electromagnetic loads and inertia loads;
- Include the geometry of the antenna that will be bolted to the bosses;
- Update the geometry with the weld shape that better represents the reality;
- Repeat the same fatigue assessment in the weld root and weld toe;
- Extend the study to the cracks originated in the weld root and propagated through the weld material to ensure the welded joints reliability;
- Improve the geometry to meet the same requirements.

References

[1] “History of Fatigue - Siemens PLM Community.” [Online]. Available: https://community.plm.automation.siemens.com/t5/Testing-Knowledge-Base/History-of-Fatigue/ta-p/386364. [Accessed: 06-Oct-2018].

[2] S. Stewart, *Air disasters.* Arrow Books, 1988.

[3] G. Baylac and D. Koplewicz, “EN 13445 ‘Unfired pressure vessels’ Background to the rules in Part 3 Design,” *Design*, no. 2, 2004.

[4] R. Budynas and K. Nisbett, *Shigley’s Mechanical Engineering Design*. 2011.

[5] D. Dubina, “Introduction to Fatigue,” *Adv. Des. steel Compos. Struct. Struct.*, p. 3, 2007.

[6] K. Rege and H. G. Lemu, “Fatigue crack propagation,” *IOP Conf. Ser. Mater. Sci. Eng.*, vol. 276, p. 012027, Dec. 2017.

[7] T. Gomes, “Estudo numérico da propagação de fendas de fadiga num aço de alta resistência,” 2017.

[8] P. Chambel Jorge Pires, “Propagação de fendas por fadiga quando sujeitas a carregamentos em Modo I ou Modo III,” p. 208, 2014.

[9] “Fatigue failure (LEFM): Part Two :: Total Materia Article.” [Online]. Available: https://www.totalmateria.com/page.aspx?ID=CheckArticle&site=kts&LN=PT&NM=299. [Accessed: 03-Oct-2018].

[10] A. J. Kulazi, “Comportamento À Fadiga Do Aço Dp600,” p. 85, 2007.

[11] “What is a SN-Curve? - Siemens PLM Community.” [Online]. Available: https://community.plm.automation.siemens.com/t5/Testing-Knowledge-Base/What-is-a-SN-Curve/ta-p/355935. [Accessed: 09-Oct-2018].

[12] “High and Low-cycle fatigue.” [Online]. Available: https://www.researchgate.net/post/Should_we_use_yield_strength_or_ultimate_tensile_strength_in_fatigue_test_for_metallic_material_Why_What_is_the_minimum_load_level_we_need_to_use. [Accessed: 09-Oct-2018].

[13] “What is residual stress? - Quora.” [Online]. Available: https://www.quora.com/What-is-residual-stress. [Accessed: 05-Oct-2018].

[14] F. Makita and V. Maria, “ESTUDO SOBRE A CURVA S-N E O GRÁFICO DE WEIBULL PARA ANÁLISE DE RESISTÊNCIA À FADIGA DE CONTATO DE ENGRENAGENS,” 2011.

[15] “Endurance limit - Fatigue of Metals :: Total Materia Article.” [Online]. Available:

https://www.totalmateria.com/page.aspx?ID=CheckArticle&site=kts&NM=282. [Accessed: 09-Oct-2018].

[16] "The Goodman-Haigh Diagram for Infinite Life - Siemens PLM Community.". Available: https://community.plm.automation.siemens.com/t5/Testing-Knowledge-Base/The-Goodman-Haigh-Diagram-for-Infinite-Life/ta-p/410585. [Accessed: 09-Oct-2018].

[17] J. Martinsson, "Fatigue assessment of complex welded steel structures," pp. 1–34, 2005.

[18] D. Radaj, C. M. Sonsino, and W. Fricke, "Recent developments in local concepts of fatigue assessment of welded joints," *Int. J. Fatigue*, vol. 31, no. 1, pp. 2–11, 2009.

[19] A. Chattopadhyay, G. Glinka, M. El-Zein, J. Qian, and R. Formas, "Stress Analysis and Fatigue of welded structures," *Weld. World*, vol. 55, no. 7–8, pp. 2–21, 2011.

[20] C. M. Sonsino, "Multiaxial fatigue assessment of welded joints - Recommendations for design codes," *Int. J. Fatigue*, vol. 31, no. 1, pp. 173–187, 2009.

[21] A. F. Hobbacher, "The new IIW recommendations for fatigue assessment of welded joints and components - A comprehensive code recently updated," *Int. J. Fatigue*, vol. 31, no. 1, pp. 50–58, 2009.

[22] C. Webinar, "Fatigue of Welded Pressure Vessels • Introduction and Relevant CCOPPS Activity," *Agenda*, no. May, pp. 00-16, 2008.

[23] "R. Lara, 'ANÁLISE DE CONCENTRAÇÃO DE TENSÕES EM JUNTAS SOLDADAS', 2016," 2016.

[24] A. Lee, A. Martin, J. M. Martinez, V. Udintsev, and M. Walsh, "Fatigue assessment of standarized bosses to the VV INNER shell walls," 2017.

[25] G. R. Kumar, "Fatigue Design of Welded Connections for," pp. 19–31, 2005.

[26] J.-M. Lee *et al.*, "Comparison of hot spot stress evaluation methods for welded structures," *Int. J. Nav. Archit. Ocean Eng.*, vol. 2, no. 4, pp. 200–210, 2010.

[27] B. Giraud, J. M. Martinez, and M. Walsh, "Guideline for the fatigue assessment of Diagnostic attachments to VV welds," 2015.

[28] I. O. Dg and C. O. O. Ted, "Annex6 Fatigue assessment of OVC boss welded attachments to the VV Appendix justifying the protection against fatigue damage of OVC attachment welds to the," 2016.

[29] "The ITER Tokamak". Available: https://www.iter.org/mach. [Accessed: 10-Oct-2018].

[30] "Quadratic mesh element." [Online]. Available: https://www.sharcnet.ca/Software/Ansys/15.0.7/en-us/help/ans_elem/Hlp_E_SOLID186.html. [Accessed: 02-Oct-2018].

Attachments

Attachment 1 – Converting displacement files

```
% read file using a comma delimiter and ignoring the first two lines
M1=readtable('PLASMA_REV1.csv','Delimiter',',','HeaderLines',2);
% strip trailing spaces from the third column
M1{:,'Var3'}=strip(M1{:,'Var3'});
% get the size of the data table
s1=size(M1);
% ignore the last line
M1=M1(1:s1(1)-1,:);
% sort the data table using the second row
SM1=sortrows(M1,'Var2');


SM2=readtable('Nos_Fronteira.csv','HeaderLines',0);




i=1;
j=1;
k=1;

while true

    %número do nó
    WBM(i)=SM1{j,2};
    i=i+1;

    %coordenadas do nó
    WBM(i)=SM2{k,2};
    i=i+1;
    WBM(i)=SM2{k,3};
    i=i+1;
    WBM(i)=SM2{k,4};
    i=i+1;

    %deslocamentos do nó
    WBM(i)=SM1{j,4};  %deslocamento em x
    i=i+1;
    j=j+1;
    WBM(i)=SM1{j,4};  %deslocamento em y
    i=i+1;
    j=j+1;
    WBM(i)=SM1{j,4};  %deslocamento em z
    if j<115932
        i=i+1;
        j=j+1;
        k=k+1;
    elseif j==115932
        break
    else
        disp('Erro na leitura do final de SM1');
```

```
        break
    end
end



% write to disk the sorted data table without the variable names
writetable(SM1,'PLASMA_REV1_sorted.csv','WriteVariableNames',false);

fid = fopen('PLASMA_REV1_WB.txt','w');
fprintf(fid,'%6.2f,%19.16f,%19.16f,%19.16f,%19.16f,%19.16f,%19.16f\n',
WBM);
fclose(fid);
```

Attachment 2 – Converting temperature file

```
% read file using a comma delimiter and ignoring the first two lines
M1=readtable('PLASMA_TEMP_REV1.csv','Delimiter',',','HeaderLines',2);
% strip trailing spaces from the third column
M1{:,'Var3'}=strip(M1{:,'Var3'});
% get the size of the data table
s1=size(M1);
% ignore the last line
M1=M1(1:s1(1)-1,:);
% sort the data table using the second row
SM1=sortrows(M1,'Var2');

SM2=readtable('Nos_Volume.csv','HeaderLines',0);



i=1;    %matriz WBM
j=1;    %matriz SM1 (temperaturas) 1331990 nós
k=1;    %matriz SM2 (nós à superfície) 1339110 nós

while true

    %confirmar se o nó tem temperatura associada
    if SM2{k,1}==SM1{j,2}

        %número do nó
        WBM(i)=SM1{j,2};
        i=i+1;
        %coordenadas do nó
        WBM(i)=SM2{k,2};
        i=i+1;
        WBM(i)=SM2{k,3};
        i=i+1;
        WBM(i)=SM2{k,4};
        i=i+1;
        %valor da temperatura
        WBM(i)=SM1{j,4};

        % confirmar se estamos no final do ficheiro
        if j<1331990
            i=i+1;
            j=j+1;
            k=k+1;
        elseif j==1331990
            break
        else
            disp('Erro na leitura do final de SM');
%%%%%%%%%%%%%%%%%%%
            break
        end
    else
        k=k+1;  %próxima linha na lista global de nós de superfície
    end
end


% write to disk the sorted data table without the variable names
```

```
writetable(SM1,'PLASMA_TEMP_REV1_sorted.csv','WriteVariableNames',fals
e);

fid = fopen('Unidades [°C] PLASMA_TEMP_REV1_WB.txt','w');
fprintf(fid,'%6.2f,%12.16f,%12.16f,%12.16f,%12.16f\n',WBM);
fclose(fid);
```